pollutants

MDPI

Article

Aqueous Adsorptive Removal of Bisphenol A Using Tripartite Magnetic Montmorillonite Composites

Okon E. Okon [1,2], Edu J. Inam [1,2,*], Nnanake-Abasi O. Offiong [3] and Ukana D. Akpabio [1]

[1] Department of Chemistry, University of Uyo, Uyo 520001, Nigeria; okonokon100@gmail.com (O.E.O.); ukanaakpabio@uniuyo.edu.ng (U.D.A.)
[2] International Centre for Energy and Environmental Sustainability Research (ICEESR), University of Uyo, Uyo 520001, Nigeria
[3] Department of Chemical Sciences, Topfaith University, Mkpatak 530109, Nigeria; no.offiong@topfaith.edu.ng
* Correspondence: eduinam@uniuyo.edu.ng

Abstract: The adsorption of bisphenol A into untreated montmorillonite clay, doped titanium composite and cationic polymer modified tripartite magnetic montmorillonite composite was investigated under different conditions. The magnetic property of the modified adsorbent was ascertained by action of external magnetic field on the materials when dispersed in aqueous media. The XRD results for the unmodified and modified adsorbents showed that interlayer spacing of the clay material increases due to intercalation of the precursor molecules. The textural properties of the adsorbents from BET analysis showed that pore size and specific surface area of the tripartite magnetic composite was calculated to be 288.08 m^2/g while that of the unmodified clay was 90.39 m^2/g. The TGA results showed the tripartite magnetic composite was more stable with the lowest percentage mass loss compared to the unmodified montmorillonite. The tripartite magnetic composite showed higher adsorption capacity. Adsorption was best described by the Freundlich isotherm model, which confirmed that the adsorption process was multilayer coverage unto the uneven surface of the adsorbents. Kinetic treatment of the adsorption data confirmed the the process followed a pseudo-second-order kinetic model and predominantly chemisorption process. The standard Gibb's free energy computed for the adsorbents showed that the adsorption processes were favourably spontaneous with highly negative energy values of −336.70, −533.76 and −1438.38 KJ/mol, respectively, for the unmodified montmorillonite, doped titanium composite and the tripartite magnetic composite. It was observed that the addition of cationic aromatic moiety to the clay material increased pollutant-adsorbent interactions and improved adsorption capacity for micro-pollutants in a simulated industrial effluent.

Keywords: tripartite magnetic montmorillonite; bisphenol A; adsorption; simulated industrial effluents

Citation: Okon, O.E.; Inam, E.J.; Offiong, N.-A.O.; Akpabio, U.D. Aqueous Adsorptive Removal of Bisphenol A Using Tripartite Magnetic Montmorillonite Composites. *Pollutants* **2022**, *2*, 363–387. https://doi.org/10.3390/pollutants2030025

Academic Editor: Panagiotis Karanis

Received: 18 January 2022
Accepted: 7 April 2022
Published: 1 August 2022

1. Introduction

Decontamination of industrial effluents before disposal is a necessary step in the industrial process for removal of toxic pollutants for the preservation of the environment and ecosystems [1,2]. Emerging organic contaminants (EOCs) in industrial effluents mostly in developing countries are receiving little or no attention with respect to the method and technology for their remediation and removal [3]. Most of these emerging contaminants are known carcinogens and endocrine disruptive chemicals (EDCs) with toxic consequences on living components of the ecosystem [4]. Bisphenol A (BPA) is an endocrine disruptive compound used as plasticizers in manufacturing of many plastic materials such as polycarbonates, polyurathanes and some phenol resins [5]. Hence, BPA exists in water bottles, food cans, thermal receipts, electronic equipment, medical devices, toys, etc. Their presence in effluents can result in health complications even at very low concentration if not remediated [6]. As a lipophilic and low biodegradable chemical, BPA accumulates in the body fat of aquatic and terrestrial animals. BPA is associated with bio-accumulative

persistence and toxicity. The phenolic estrogenic BPA is among the most frequently detected emerging organic pollutants in various aqueous matrices in Africa and many other regions of the world [7–11]. Concerns about BPA contamination are mainly based on its endocrine disrupting activities and reproductive toxicity on living systems, including humans [6]. The discharge of such effluent into water bodies and the environment results in accumulation in the biota and hence its health and ecological consequences [12]. Due to a lack of regulations in developing countries for these emerging contaminants in the environment, their presence in the environment is sometimes ignored, hence the need to develop local and cost-effective technology for remediating these wastes for environmental sustainability. Again, in the industries, water is an important material input and accounts for over 10% of the cost of production in some companies [13]. Water reusability leading to reduced cost of water consumption can be enhanced through efficient effluent treatment technology. Some approaches developed for remediation of BPA in water include: laccase-catalysed degradation [14], advanced oxidation process using zero-valent iron activated persulphate system [15–18], degradation using TiO_2 photocatalysis with ozone [19–23], enzymatic remediation using biosurfactants [24], removal using electro-Fenton process [25], adsorption [26], oxidation using UV-C/peroxymonosulphate system and mineralization using integrated ultrasound-UV-Fe(II) treatment [27,28]. Also, some microorganisms such as fungi and bacteria have been shown to have a degradation effect on some pollutants [29]. Specifically, some experiments on degradation of BPA by microorganisms by some strains of fungi and bacteria have been reported [30,31]. Many of these methods are expensive and cannot be applied in developing countries. Others, such as conventional coagulation methods and chemical precipitation, cause secondary contaminants, requiring an additional treatment and increasing the treatment cost [32]. Interestingly, adsorption is the most attractive process in developing countries due to its lower cost and high efficiency in removing different types of contaminants. Many reports on modified clay for removal of BPA were focused on metal nanoparticles; however, some research on use of cationic surfactants and polymers has also been reported in literature [5,13,33–35]. These include the use of multi amine-containing Gemini surfactant as organic modifiers for montmorillonite clay [13] and the use of cetyl trimethyl ammonium bromide (CTAB) for modification of magnetic bentonite [33]; also, clays modified using octadecyltrimethylammonium bromide (ODTMA, organic modifier) and hydroxy aluminium (Al_{13}, inorganic modifier) [36]; use of dodecyltrimethylammonium, tetradecyltrimethylammonium, hexadecyltrimethylammonium, and didodecyldimethylammonium, at different concentrations into two natural clays from Burkina Faso [37]; use of hexadecyltrimethylammonium bromide (HS) and alkyldimethylbenzylammonium chloride [38]; use of Titanium (IV) tetra-iso-propoxide and cetyltrimethylammonium (CTA) [39]; use of dodecyldimethyl 3-sulphonate, dodecyldimethyl N-carboxylate and dodecyldimethyl N-phosphate [40] have been reported in literature. However, most of these organic modifiers are non-biodegradable and may persist in the environment, thus resulting in secondary pollution [41]. Also, metal composites without supportive components display serious shortcomings during application such as agglomeration, limited reusability, and non-biodegradability, resulting in further contamination of the environment [42,43]. Additionally, surfactants lack mechanical and thermal stability, as well as low adsorptive efficiency. In order to overcome these limitations, researchers have developed clay-polymer nanocomposites (CPNs) combining the advantageous characteristics of both clay minerals (cheapness, availability, eco-friendly, large surface area and stability) and polymers (mainly the high adsorption efficiency, high surface area and better regeneration) [44,45]. Interestingly, CPNs showed advanced properties (mechanical strength, low gas permeability and heat resistance) allowing cost reduction and enhancing their efficiencies in removing various contaminants from water. In addition, many of these CPNs can be synthesized from green materials, which are considered sustainable [46]. Some polymeric modifiers loaded on clay have been reported including cationic polyacrylamide [5], sulfonated polystyrene [3] and resorcinol-formaldehyde polymer blend [47]. However, these polymer-clay nanocomposites (PCNs) were synthesized

and applied for wastewater treatment containing mostly of dyes, phenols and other organic pollutants such as pesticides. Another setback of engineered clays for adsorption has to do with their recovery from effluent stream. The introduction of magnetic particles into the composite matrix can enhance its recovery using an external magnetic field as demonstrated in this work. Hence, the use of a polymeric biodegradable cationic organic moiety with positive N-group to facilitate adsorption of BPA from a simulated industrial effluent through increased electrostatic interaction and hydrophobic attraction is reported in this paper.

The main objective of this work was to examine the adsorption capacity of a tripartite magnetic montmorillonite composite modified by doped titanium oxide and polymeric cyclodextrin-toluenediisocyanide alt-polymer with positive N- head group as biodegradable organic moiety to improve the efficiency of the clay material for adsorption of BPA from simulated industrial effluents.

2. Materials and Methods

Montmorrilonite clay was obtained from deposits in Itu, Nigeria, which has been previously identified as montmorilonite type clay at Soil Science Department, University of Uyo, Uyo, Nigeria [48]. Beta cyclodextrin, toluenediisocyanate, dimethyl sulfoxide, were from Siqma Aldrich, Milwaukee, WI, US. Acetone, ethanol, SDS, were from Merck, Darmstadt, Germany. $FeCl_2 \cdot 5H_2O$, $FeCl_3 \cdot 6H_2O$, NH_4OH, and NaOH were obtained from Double Bond Chemicals, Uyo. BPA was obtained from Xiya Chemicals Manufacturing, (Shandong, China). $NiCl_2$.5H2O, $PbSO_4$.H_2O and $CdCl_2$.H_2O were of analytical grade from Merck, Darmstadt, Germany. All other reagents were of analytical grades and were used without further purification.

2.1. Characterization of Composite

Surface morphologies of the parent and composite materials were deduced using Scanning Electron Microscope (SEM) at University of Cape Town, South Africa. Surface area and pore parameters, crystallinity and functional group were deduced using BET surface analyzer (Micromeritics), X-ray Diffraction spectroscopy and Fourier-Transformed Infrared (FTIR) spectroscopy, Energy dispersion spectroscopy, Scanning electron microscopy and thermogravimetry.

2.1.1. Nitrogen Adsorption–Desorption Measurements

Nitrogen adsorption–desorption measurements (BET method) was measured using exactly 1 g each of MM, DT-Fe@MM and nCDp/DT-Fe@MM samples at liquid nitrogen temperature (−196 °C) and relative pressure Po/P between 0.01–1.00 with an autosorb BET apparatus, Micromeritics ASAP 2020, surface area and porosity analyzer. The analysis procedure is automated and operates with static volumetric technique. Before each measurement, the samples were first degassed by heating at 200 °C for 2 h according to the method of Liu et al. [49].

2.1.2. X-ray Diffraction (XRD)

The bulk structure of both parent clay and the modified clay composites were confirmed by X-ray Diffraction (XRD). X-ray diffraction data of the obtained materials were obtained by a Bruker D8 Advance powder X-ray diffractometer (Bruker, Munich, Germany) of Cu Ka radiation with a step size of 0.028 at a rate of 17.7 s $step^{-1}$ from 2° to 60° according to the method of Liu et al. [49].

2.1.3. Fourier Transformed Infrared (FTIR)

The determination of the surface functional groups was carried out using FTIR spectrophotometer (Fisher Thermoscientific, Waltham, MA, USA) following standard procedures. The spectra were recorded using KBr wafers in the range 4000 cm^{-1} to 400 cm^{-1} according to the method of Men et al. [5].

2.1.4. Scanning Electron Microscope (SEM)

The Scanning Electron Microscope (SEM: JSM-5310LV Microanalyzer, JEOL Co., Tokyo, Japan) was employed to determine the surface morphology of catalysts according to the method of Men et al. [5].

2.1.5. Thermogravimetric Analysis

The Thermogravimetric data were recorded on a TGA-50 (ASCII-Microanalyzer, JEOL Co., Tokyo, Japan) at a temperature range of 19.7 °C to 999.91 °C and sample mass of 10.285 mg over acquisition time of about 10 h and nitrogen flow rate of 50 mL/min on a platinum macro pan according to the method Liu et al. [50].

2.2. Preparation of Magnetic Montmorillonite

Montmorillonite was converted to its magnetic form following the modified method of Cao et al. [33]. Briefly, about 10.0 g MM in 100 mL deionized water and left to stabilize for 5 h at 50 °C. $FeCl_2 \cdot 6H_2O$ (8.6 g) and $FeCl_3 \cdot 7H_2O$ (12.8 g) were then added and stirred vigorously for 1 h at 70 °C followed by addition of 28% NH_4OH in drops and the pH was adjusted to 10 using dilute NaOH. Mixture was filtered; the solid particles were washed with deionized water and Ethanol and dried then at 80 °C for 12 h. The resulting product was named Fe@MM.

2.3. Preparation of Doped Titanium Magnetic Montmorillonite

The doped titanium component was prepared using the modified method of Cao et al. [33]. Briefly, about 2 g TiO_2 and STS in a 16 v/v acetone solution and ethylenediamine was added at 70 °C and stirred in an autoclave for 2 h to form a sol-gel. This was added to a 5 g solution of Fe@MM in acetone and stirred magnetically for another 30min with addition of 0.22 M NaBH4 in drops. The mixture was centrifuged for 30min, and the obtained solid was dried at 80 °C for 12 h and labelled as DT-Fe@MM.

2.4. Preparation of β-Cyclodextrin Nano-Polymer and Composite Blending

To prepare the β-cyclodextrin-toluenediisocyanide alternating nanopolymer, about 10 g of β-CD was added to 15 v/v acetone in deionized water and stirred vigorously for 1 h. TDI was added in drops and the solution was stirred at 50 °C. It was then poured into a stream of acetone, and the precipitate was separated and washed with acetone and deionized water and dried in a vacuum desiccator for 12 h, labelled as nCDp. Blending of the different components to form the tripartite composite was as follows: about 5.5 g of DT-Fe@MM was dispersed in DMSO and stirred magnetically for 4 h, followed by addition of 1.8 g of nCDp and 2.2 g of SDS at 70 °C with continuous stirring for another 1 h. The mixture was then centrifuged at 3600 rpm for 30 min, and the obtained solid was dried at 110 °C with further calcination at 550 °C for 6 h. The product was labelled nCDp/DT-Fe@MM. The preparation of the tripartite magnetic montmorillonite composite can be represented by the schematic diagram in Figure 1.

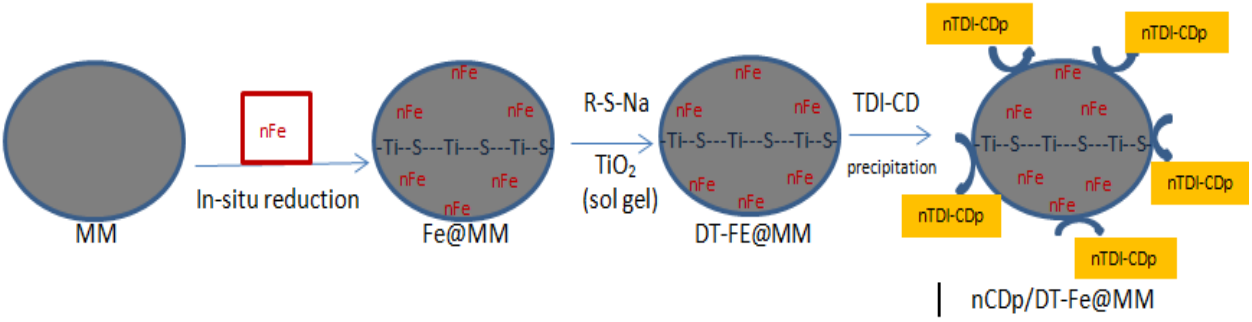

Figure 1. Schematic representation of the preparation steps of the tripartite magnetic montmorillonite composite.

2.5. Batch Adsorption Studies

Exactly 0.2 g of unmodified montmorillonite doped titanium composite and the prepared tripartite magnetic composite was added to about 20 mL of simulated effluent at varying concentrations of 10, 20, 40 and 50 mg/L in a conical flask and covered with aluminum foil. The conical flask was agitated on a platform shaker at 360 rpm for 90 min. The mixture was then filtered and stored in glass vials for analysis. The adsorption process was repeated by varying temperature range from 30–70 °C and varying the pH range between 3–12. The concentration of BPA was analysed by ultraviolet-visible spectrophotometry while metals concentration was analysed by atomic absorption spectrophotometry. The removal efficiency and adsorption capacity of the different adsorbents was calculated using Equations (1) and (2), respectively. The mechanism of adsorption was studied using four adsorption models, namely, Langmiur, Freundlich, Florry-Huggins and Dubinin-Radushkevich isotherms.

$$\% \text{ adsorption} = (1 - \frac{C_e}{C_o}) \times 100\% \quad (1)$$

$$q_e = \frac{(C_o - C_e)}{m} \times \frac{V}{1000} \quad (2)$$

where C_o and C_e represent the initial and equilibrium concentration of micro-pollutants in solution (mg/L), q_e is the equilibrium adsorption capacity of the adsorbents, V (L) is the volume of simulated effluent used and m is the mass (g) of adsorbent used.

2.6. Desorption Experiment

To measure the rate of desorption of the adsorbate in acetone and deionized water after adsorption, 2.0 g of the residue obtained from the adsorption experiment was dispersed in 40 mL of acetone and deionised water in two different conical flasks. The resultant solution was then agitated between 0–120 min at different time intervals, filtered and the percentage desorption was calculated using Equation (1).

2.7. Preparation of Simulated Effluents

Stock solution of BPA was prepared by dissolving 0.5 g of the compound in 500 mL deionised water to obtain 100 µg/mL. Lower concentrations was prepared from the stock solution using dilution principle. A total of 100 µg/mL each of solutions of cadmium, lead and arsenic salts were prepared by dissolving 0.05 g of $CdCl_2$, $Pb(NO_3)_2$ and $AsCl_3$ in 1000 mL of deionised water, respectively. An equal proportion of each of the solutions of the micropollutants were mixed together to obtain the simulated industrial effluents; the resultant pH of the solution was 5.7 and the net ionic strength was about 0.01 M.

3. Results and Discussion

3.1. Magnetic Property of Modified Composite

The modified composite was dispersed in a solution and its magnetic property was examined using an external magnetic field. The composite was attracted by an external magnetic field and was separated from the solution using a magnet, as shown in Figure 2.

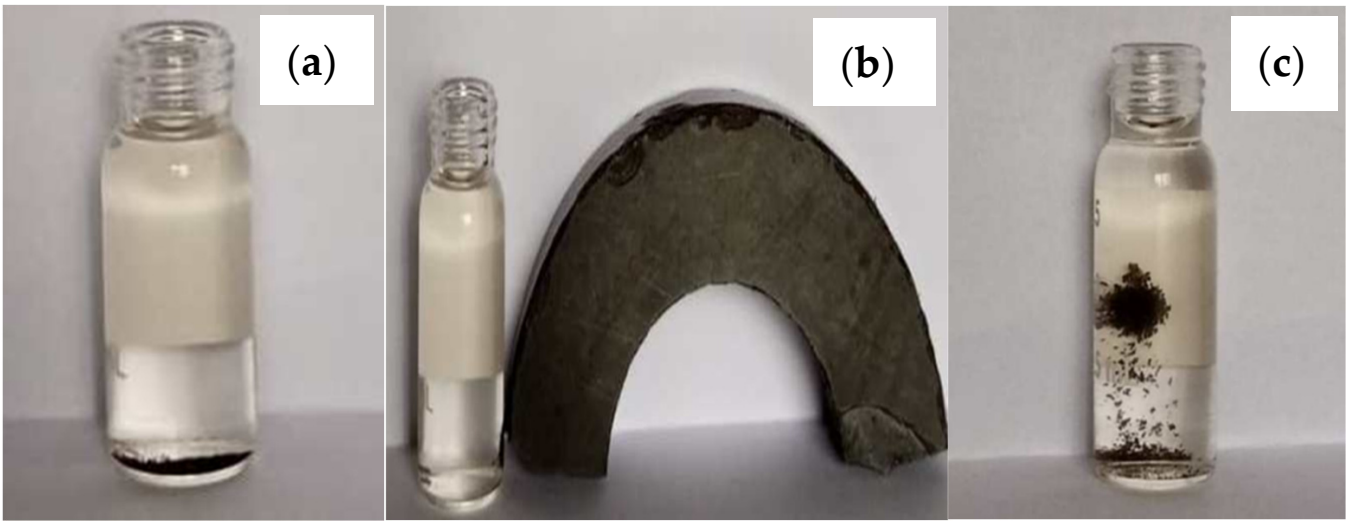

Figure 2. (**a**) nCDp/DT-Fe@MM without external magnetic field, (**b**) nCDp/DT-Fe@MM particles attracted to an external magnetic field, (**c**) nCDp/DT-Fe@MM particles in solution carried by an external magnetic field placed behind it.

3.2. UV-Visible Calibration Curve of Absorbance of BPA from Solution

The calibration curve for UV-visible absorbance to concentration plot for the BPA at 278 nm is presented in Figure S1 (Supplementary Material). The calibration plot shows an almost perfect fitting with R^2 value of 0.995, showing the high sensitivity of the equipment for accurate determination of BPA concentration in the simulated and pretreated samples. Other instrumental quality parameters were adjusted according to united state pharmacopia specifications. The phtometric accuracy was adjusted in the operational wavelength region using potassium dichromate solution (60 mg/L, 80 mg/L and 160 mg/L) and solutions standard accordingly. Also, wavelength acuracy and precision in the region of 240–650 nm was set using a holmiun oxide solution. Since the ionic strength of the simulated industrial effluent prepared using deionised water was relatively low, its matrix effect on the measurement of bisphenol concentration using uv-vis spectrophtometer could be accounted for using the standard calibration curve.

3.3. Functional Group Characterization of the Prepared Adsorbents

The FT-IR spectra of the raw montmorillonite (MM) and the functionalized composites are shown in Figure 3a–c. The raw montmorillonite showed mostly -OH, Si-O and Al-O peaks at 3623, 998, and 749 cm^{-1}, respectively. The modified montmorillonite not only has the characteristic peak of MM but also shows new peaks, which proves that the chemical structure of the modified composites has changed. The sulphur doped titanium composite showed peaks for -NCS (isocyanate) at 1990 cm^{-1} and the organic modified composite showed peaks for open chain azo (-N=N-), cyanide (-OCN), and transition metal carbonyl (-M=CO-) at 1032, 1625 and 2050 cm^{-1}, respectively. This new peak showed functionalization of the composites occurred and that sulphur, titanium and the isocyanate-cyclodextrin biodegradable polymer were intercalated into the montmorillonite framework [3,5,51,52].

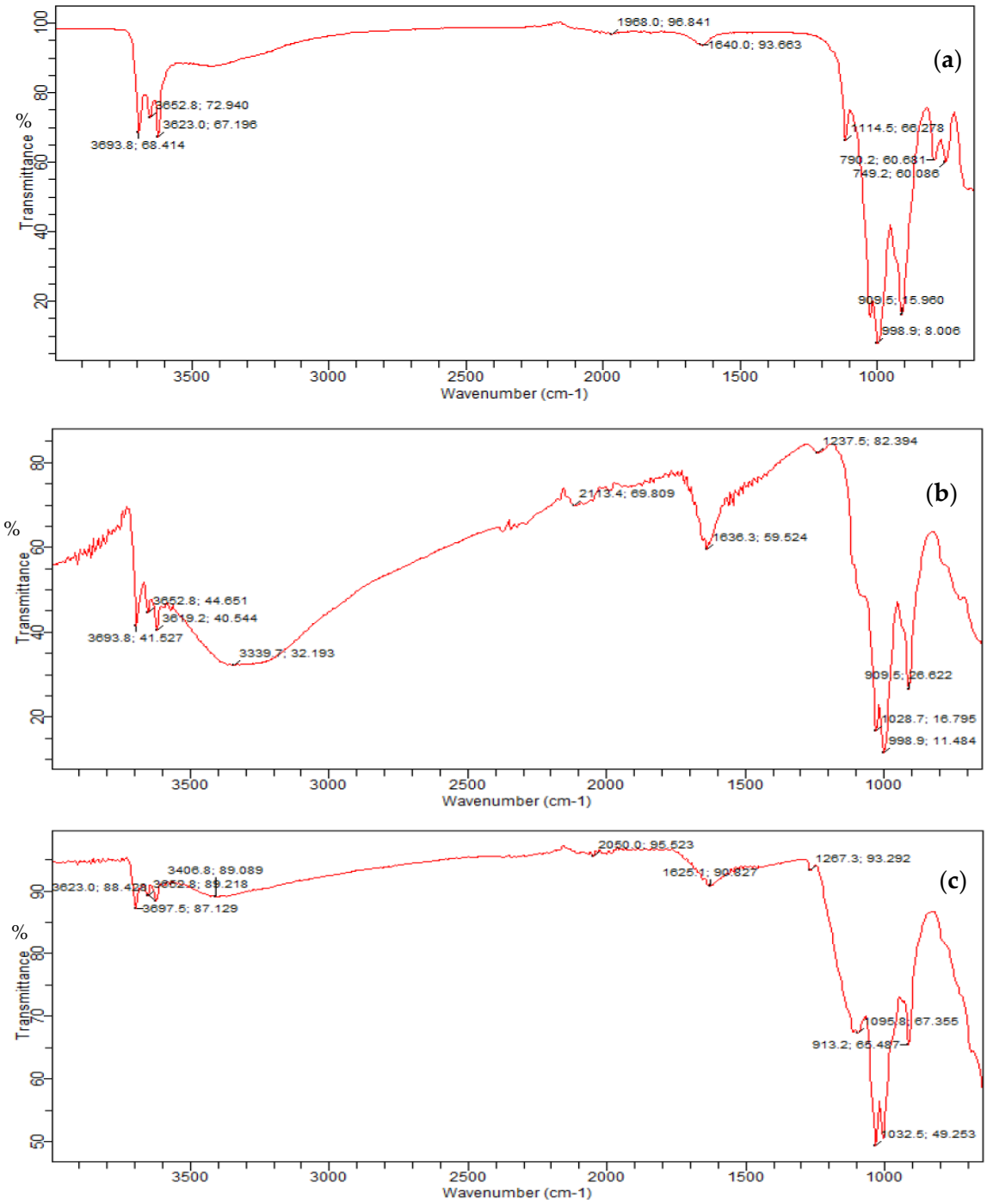

Figure 3. FT-IR spectra of the (**a**) raw montmorillonite (MM), (**b**) doped titanium composite and (**c**) the tripartite magnetic composite.

3.4. Scanning Electron Microscopy

The scanning electron microscopy (SEM) showing the surface morphologies of the raw clay, titanium doped clay and the tripartite magnetic nanocomposites are presented in Figure 4a–c, respectively. The surface of the raw clay showed a typical flat and flaky morphology compared to the doped titanium composited whose morphology became a thin layer structure with fluffy appearance after the modification. The tripartite composite showed further smaller flakes and a more loosed structure showing also the appearance of submicron sized globules of the polymeric organic modifier on the montmorillonite surface [53].

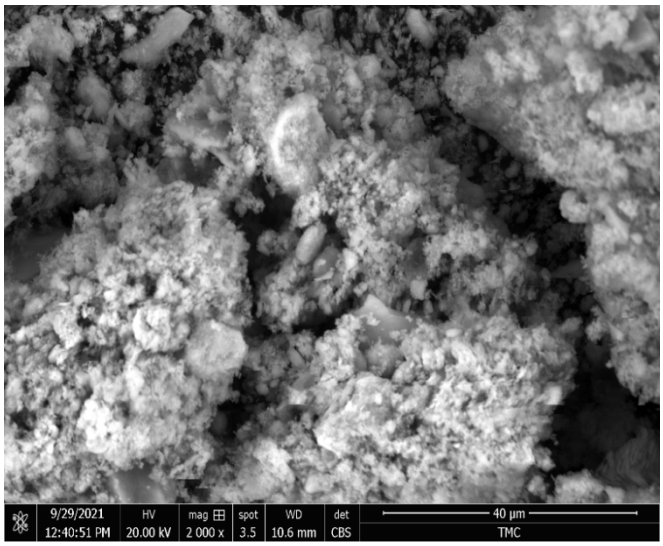

(**a**)

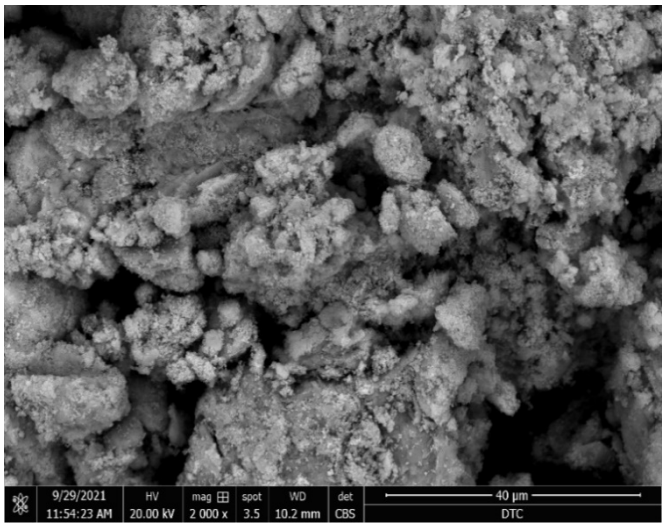

(**b**)

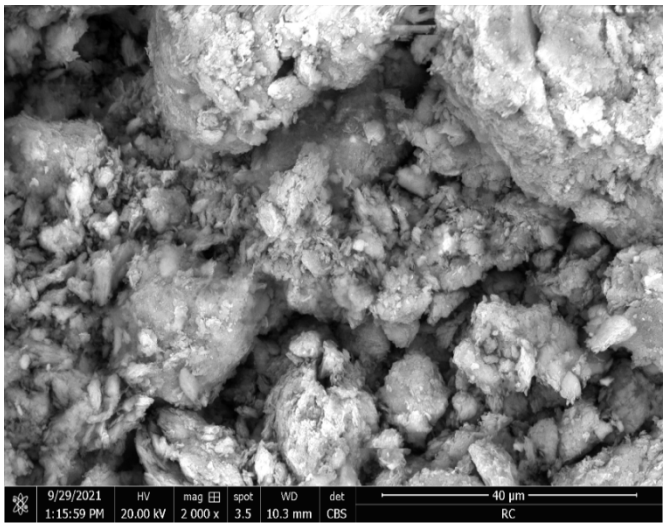

(**c**)

Figure 4. (**a**–**c**): SEM images of raw clay (MM), doped titanium composite (DTC) and the tripartite magnetic nancomposites (TMC) showing their surface morphologies.

3.5. X-ray Diffraction Patterns of Studied Materials

The X-ray patterns of the unmodified montmorillonite (RC), doped titanium composite (DTC) and the tripartite magnetic montmorillonite composite are depicted in Figure 5a–c. The unmodified montmorillonite showed typical peaks for clay material in the following mineral phases; Quartz at 2θ = 20.9, 26.7, 36.6 and 39.6 according to JCPDS No. 79-1906; Montmorillonite at 2θ = 54.7 and 62.3 according to JCPDS No. 03-0009; Moganite at 2θ = 19.95 according to JCPDS No. 79-2403. However, most of the peaks disappeared or were weakened on loading of the doped titanium particles and the polymeric organic moiety leaving mostly peaks for the quartz and montmorillonite at 2θ = 26.7, 36.6, 54,7 and 62.3. The raw clay also showed its first reflection (d001) peaks at 2θ = 5.26 with a d-spacing of 1.67 nm, which is typical of Ca-montmorillonite [54]. However, this peak was deflected in the doped titanium to 2θ = 5.21, corresponding to a d-spacing of 1.71 nm and confirms that the doped titanium particles were successfully intercalated into the montmorillonite layer. Unsurprisingly, in the tripartite composite, the peak was further shifted to 2θ = 20.4 and corresponds to d-spacing of 0.44 nm. This suggests that the polymeric organic moiety was rather adsorbed on the surface of the clay mineral without intercalation. The reduction in interlayer spacing in the tripartite composite could be a result of the loading of structurally bulky groups onto the clay surface or a gradual delamination of the clay framework due to high temperature calcination [33,55].

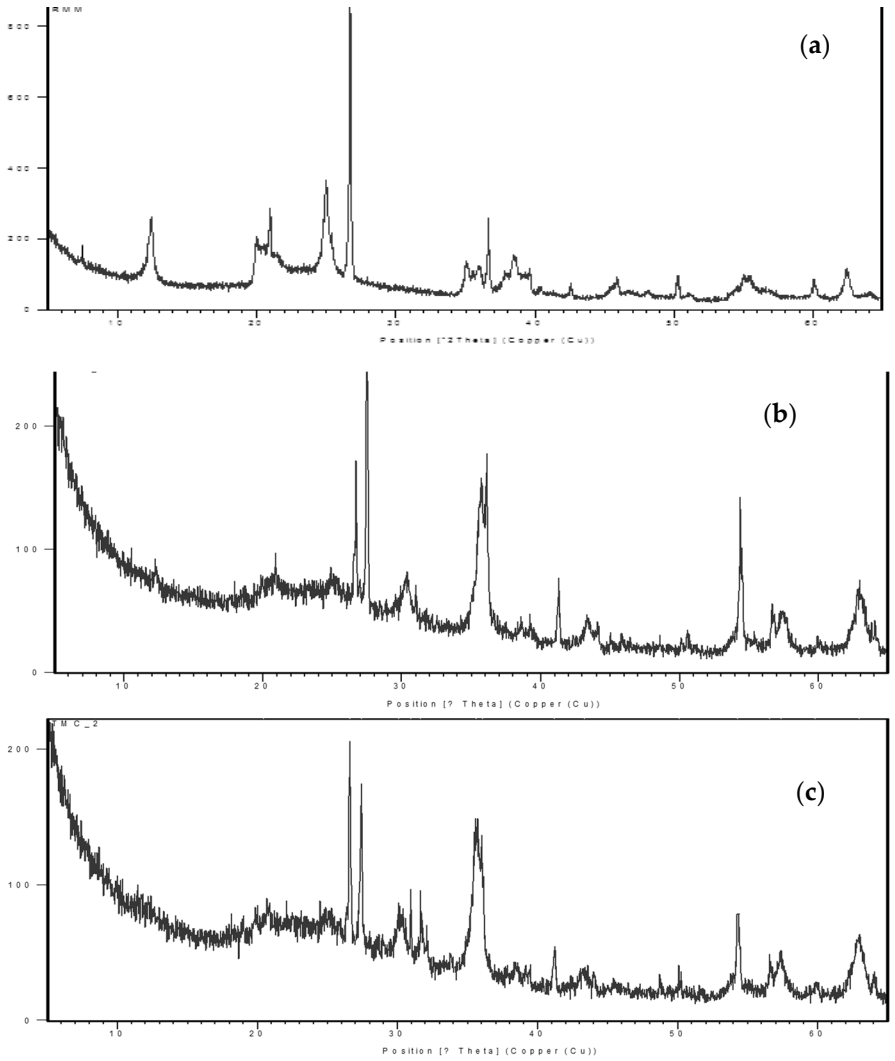

Figure 5. (**a**–**c**): XRD patterns of (**a**) unmodified montmorillonite, (**b**) doped titanium composite and (**c**) tripartite magnetic montmorillonite composite.

3.6. BET Analysis

The N_2 adsorption-desorption studies of the unmodified montmorillonite, doped titanium composite and the tripartite magnetic composite are represented in Figure 6. The raw clay according to IUPAC classification is exhibited as a type III curve and H3 hysteresis loop which indicates the presence of mesoporous materials [33]. The two modified composites exhibited a type II curve showing lower surface area for monolayer coverage in agreement with basic isotherm model predictions for the modified composites. The BET surface area for the tripartite magnetic composite was calculated to be 288.08 m^2/g, while that of the unmodified clay was 90.39 m^2/g. The increase in specific surface area with modification was due to increased sorption sites on the surface of the modified material. However, although the specific surface area of the modified composite was larger, its pore volume was smaller compared to the unmodified clay due to interlayer modification by the intercalating species. This increase in S_{BET} should be reflected in the enhancement of the adsorption capacity. A summary of textural properties of the adsorbents is presented in Table 1.

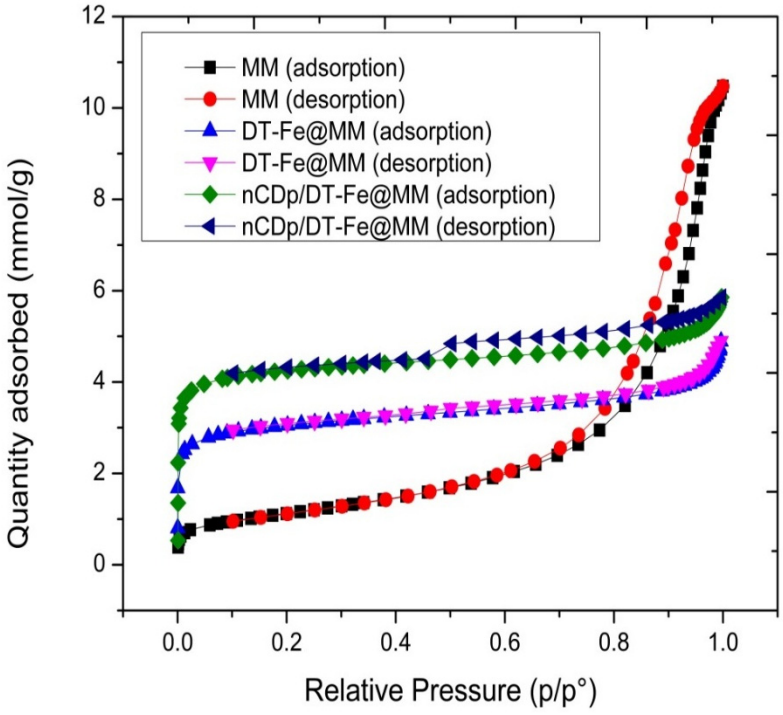

Figure 6. BET surface characterization result of unmodified montmorillonite (MM), doped titanium composite (DT-Fe@MM) and tripartite magnetic composite (nCDp/DT-Fe@MM).

Table 1. Summary of textural properties of the adsorbents from BET analysis.

Sample Name	S_{BET} (m^2/g)	Total Pore Volume (cm^3/g)	BJH-Average Pore Diameter (nm)	Pore Size (nm)	Micropore Volume (cm^3/g)
MM	90.398	0.3285	14.30	6.730	0.002729
DT-Fe@MM	210.720	0.1435	6.37	2.725	0.077269
nCDp/DT-Fe@MM	288.079	0.1907	5.69	2.648	0.113633

3.7. Thermogravimetric Analysis

The thermogravimetric analysis plot for the unmodified montmorillonite, doped titanium nanocomposite and the tripartite magnetic montmorillonite is presented in Figure 7a–c. The unmodified clay showed two stages of weight loss at a temperature between 30–150 °C and 450–600 °C, corresponding to a release of physisorped water and removal of the dehydroxylation layer inside the clay material, respectively [49]. The doped

titanium nanocomposite exhibited mass loss at 30–150 °C, 450–550 °C and above 800 °C, which were attributed to a slight removal of absorbed water, removal of the layer of dehydroxylation, and the burning of carbon residue, respectively [49,50]. For the tripartite nanocomposite, there was only negligible mass loss until a temperature of 230–400 °C was reached, which was attributed to the removal of N-groups from modifier groups [56]. Also, from the plots, the modified nanocomposites presented lower percentage mass losses (22.4 and 3.4) compared to the unmodified clay (28.1).

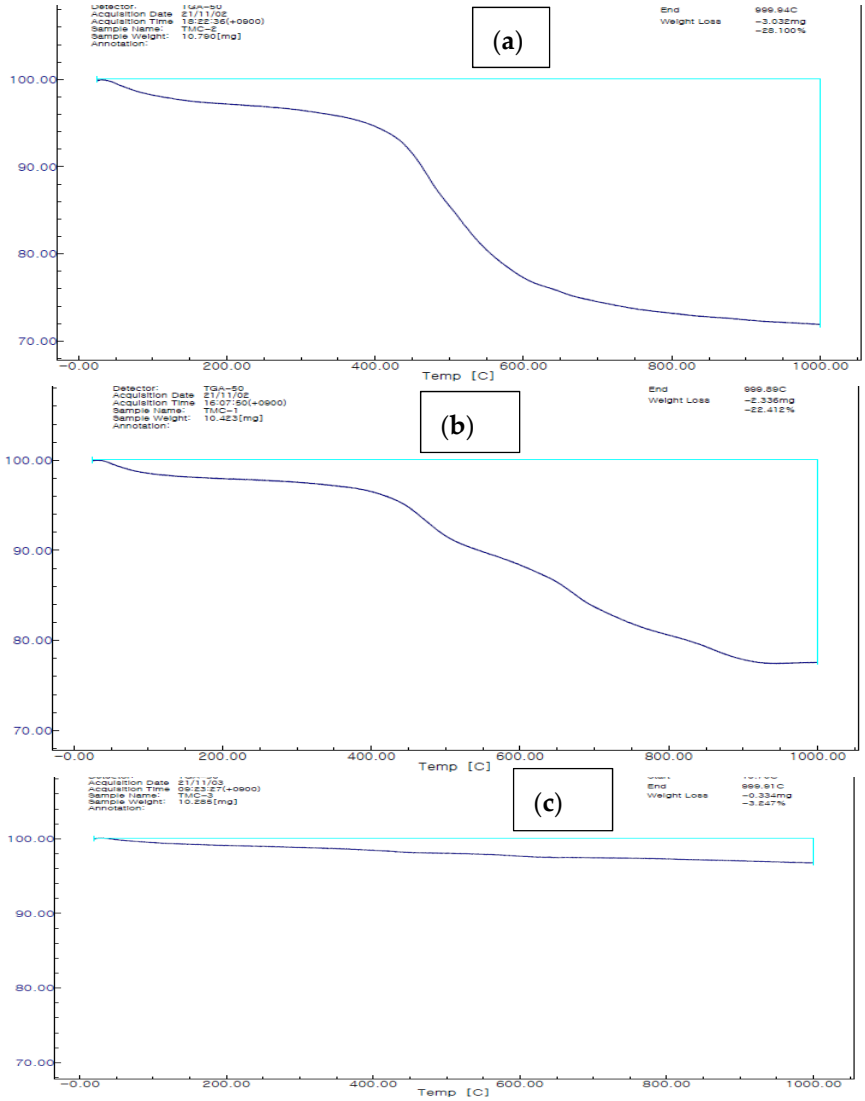

Figure 7. (**a**–**c**) Thermogravimetric analysis plot for the unmodified montmorillonite, doped titanium nanocomposite and the tripartite magnetic montmorillonite.

3.8. Zeta Potential of Unmodified and Modified Montmorillonite Adsorbents

Zeta potential of the adsorbents materials was also studied as a function of pH to ascertain the stability of the materials to coagulation in aqueous dispersion. The result of the zeta potential studies is presented in Figure 8. From the results, the zeta potentials of the materials were high, showing high stability to coagulation. Also, the isoelectric point of the materials (pzc) was defined for each adsorbent, showing that the materials were generally stable to agglomeration since their zeta potential falls outside the isoelectric point. The pzc for the adsorbents were MM (4.7), DT-Fe@MM (7.4) and nCDp/DT-Fe@MM (9.4), respectively.

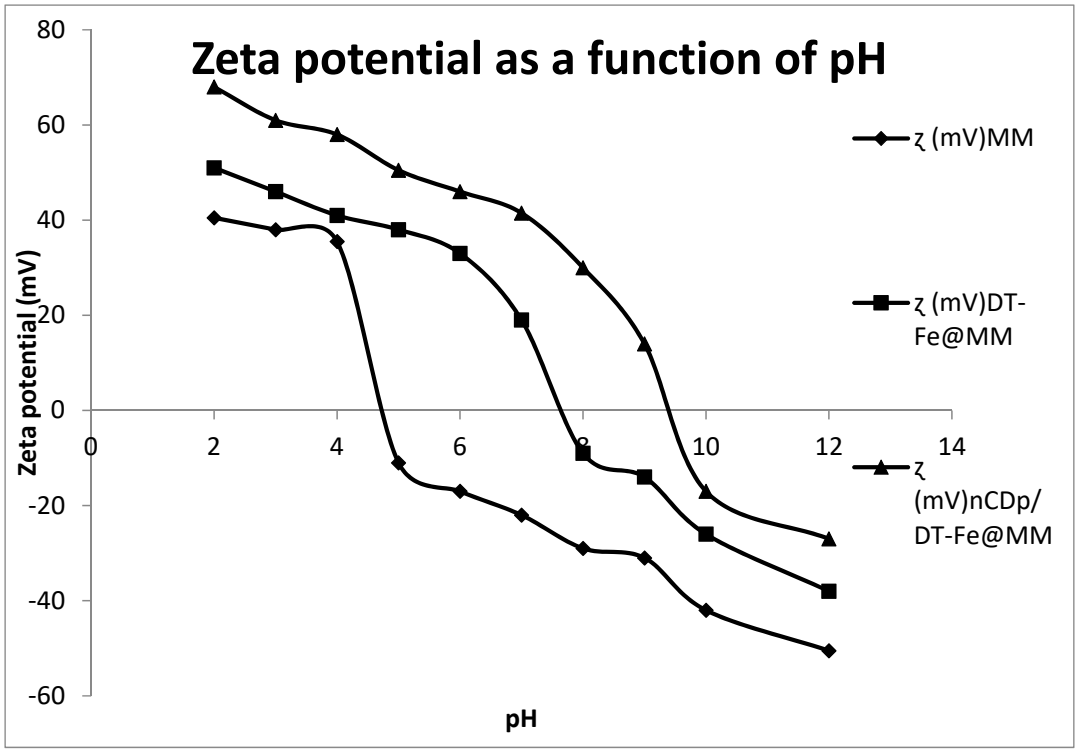

Figure 8. Zeta potential of unmodified and modified montmorillonite adsorbents as a function of pH.

3.9. Adsorption Efficiencies of Adsorbents for BPA in Simulated Industrial Effluents

The preliminary adsorption efficiency of the tripartite composite compared to that of doped titanium composite and the natural unmodified montmorillonite is depicted in Figure 9 for adsorption of BPA. With an equal adsorbent dosage of 0.02 g, it was found that the tripartite composite showed higher percentage adsorption than the other adsorbents under the same conditions.

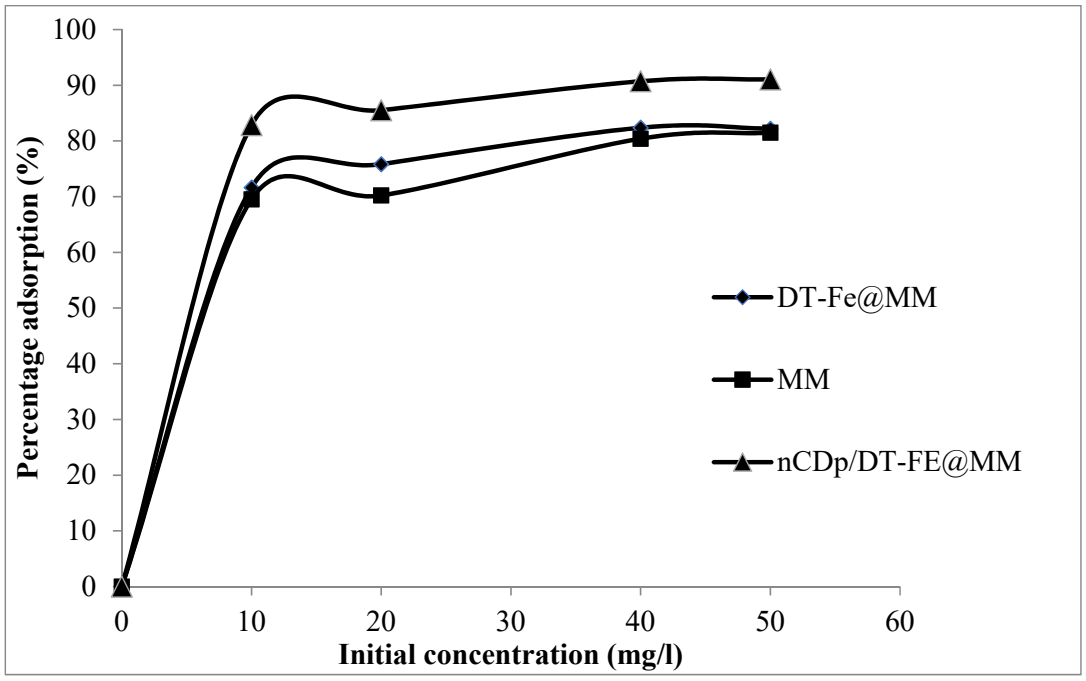

Figure 9. Percentage Adsorption of BPA unto Untreated Montmorillonite (MM), Doped titanium composite (DT-Fe@MM) and Tripartite montmorillonite composite (nCDp/DT-Fe@MM).

From the plots, it was also found that percentage adsorption increases with an increase in initial concentration of adsorbate for the composite in contrast with other adsorbent with relative decrease adsorption at higher concentration. This suggests that the composite has a higher surface area. This functionalized surface enhances better pollutant-adsorbent interactions to adsorb at higher concentration compared to other adsorbents, which are suspected to undergo slight desorption at a higher concentration due to low surface area and poor pollutant-adsorbent interactions [57–59].

3.10. Effect of Dosage of nCDp/DT-Fe@MM

Result of effect of dosage on adsorption of BPA unto nCDp/DT-Fe@MM, DT-Fe@MM and MM is presented in Figure 10. Adsorption increased with dosage and reaches equilibrium at a dosage of 0.02 g/L. Further increase in adsorbent dosage was found to exert little or no effect on adsorption capacity of the process. Higher adsorption efficiency was recorded for the tripartite magnetic composite. This was due to better functional sites and interaction forces as a result of the modifications.

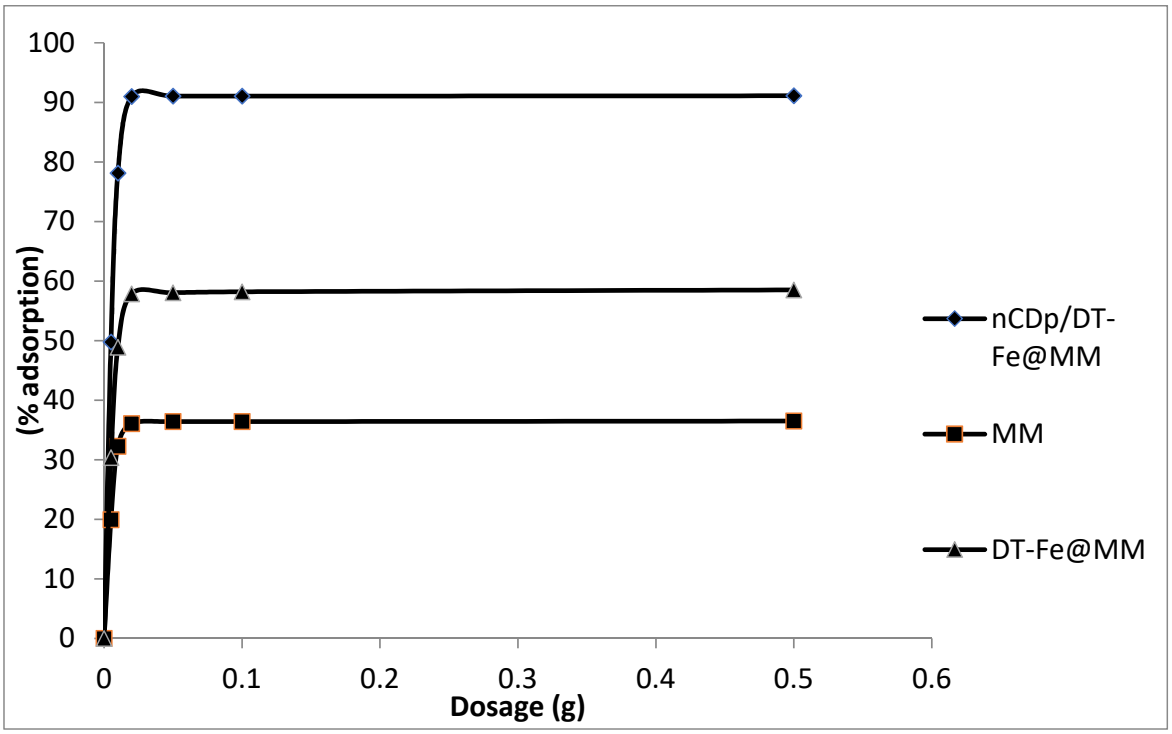

Figure 10. Effect of dosage on the removal of BPA. (Adsorption conditions: C_o 50 mg/L; T = 30 °C; t = 120 min; pH = 7).

3.11. Effect of Time on Adsorption of BPA

The variation in rate of BPA adsorption unto the three adsorbents was studied and the result is presented in Figure 11. The adsorption of BPA increased with increasing time and reaches equilibrium at 30 min with a slight change up to 90 min followed by slight decrease beyond this equilibrium time. Adsorption capacity of nCDp/DT-Fe@MM for BPA was higher than that of DT-Fe@MM and MM. Increased adsorption by the tripartite magnetic montmorillonite was due to addition of hydrophobic cyclodextrin nanopolymer with positive N-group, which increases the π-π and OH-π interactions as well as increased electrostatic interaction between BPA and the functionalized composite [5,33,59,60].

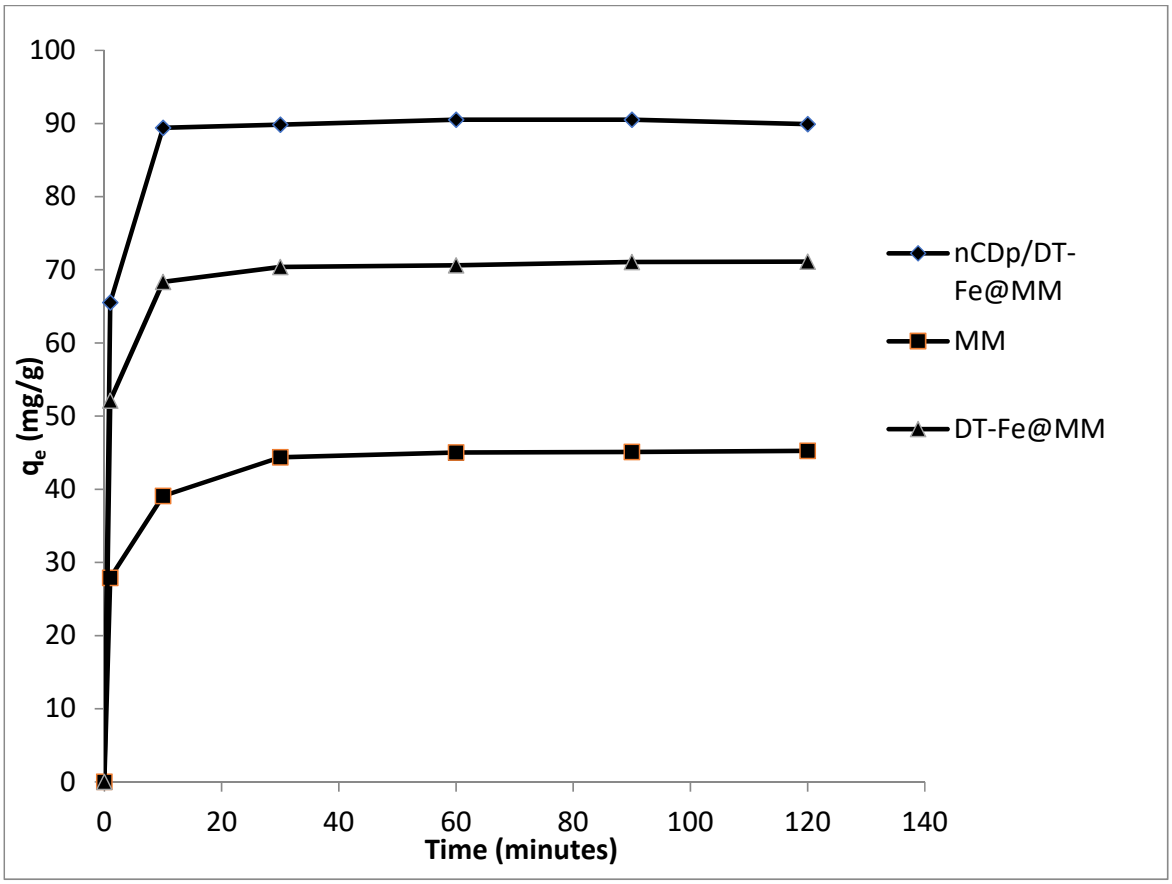

Figure 11. Effect of adsorption time on the removal of BPA. (Adsorption conditions: C_o 50 mg/L; T = 30 °C; dosage = 0.02 g/L; pH = 7).

3.12. Effect of Solution pH

The adsorption behavior of BPA under varying solution pH was studied and the result is presented in Figure 12. Solution pH has been observed to have an effect on adsorption capacity of adsorbents in such medium [5,13]. Adsorption of BPA increased with increased pH with maximum adsorption at pH 8 and thereafter began to decline at higher pH value. Similar results were observed by Cao et al. [33]. At a lower pH value, BPA, being a weak acid, exists in the protonated form and reaches first deprotonation at pH 8, thus increasing electrostatic attraction between the positive N-group of the modified adsorbent, leading to peak adsorption capacity. However, beyond a pH value of 8, the surface of the modified montmorillonite composite becomes negatively charged due to ionization of oxygen containing groups, and leading to increased electrostatic repulsion between the composite and BPA; hence, the reduction in adsorption capacity at higher pH values [13,33,61].

3.13. Effect of Adsorbent Particle Size on BPA Adsorption

The effect of adsorbent particle size on the adsorption of BPA from an industrial effluent is presented in Figure 13. Adsorption increases with particle size, with maximum adsorption occurring at 0.02 nm and thereafter began to decrease with increase in particle size. It was found that lower adsorption capacity at 0.1 nm could be due to agglomeration followed by rapid desorption [62]. Larger particle size ranging from 0.2 nm to 1 nm can resist the agglomeration effect; hence, a higher adsorption capacity is maintained.

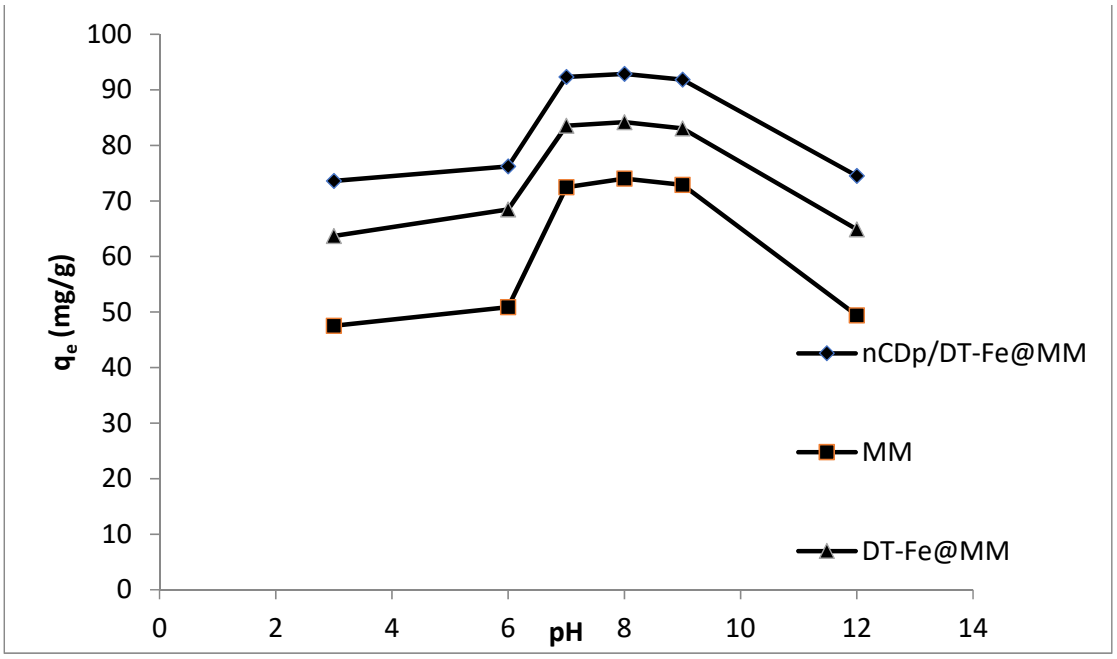

Figure 12. Effect of pH on the removal of BPA. (Adsorption conditions: C_o 50 mg/L; T = 30 °C; dosage = 0.02 g/L; t = 120 min).

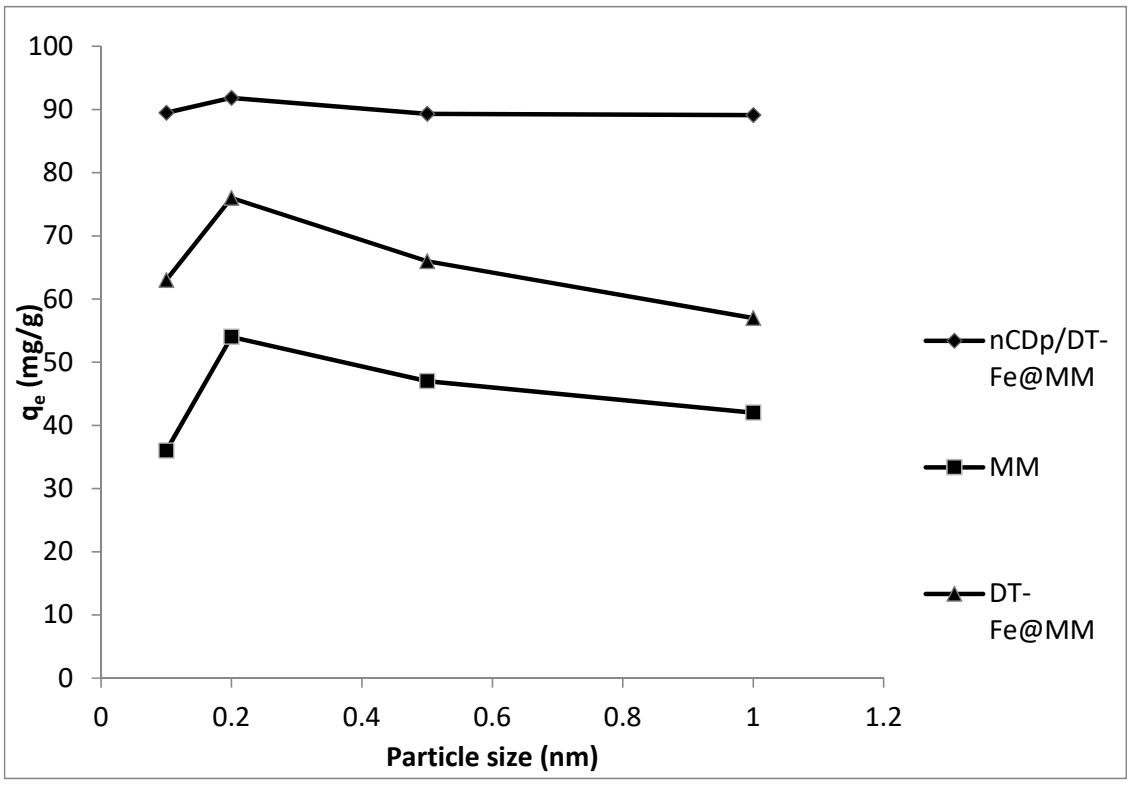

Figure 13. Effect of adsorbent particle size on the removal of BPA. (Adsorption conditions: C_o 50 mg/L; T = 30 °C; dosage = 0.02 g/L; t = 120 min; pH = 8).

3.14. Effect of Temperature on Adsorption of BPA

The result effect of temperature on BPA adsorption is presented in Figure 14. There was high adsorption recorded at room temperature and it increased and reached a maximum value at 40 °C. Thereafter, there was a decrease in adsorption as the temperature increased. It was observed that a decrease in adsorption capacity at a higher temperature could be due to energetics of the adsorption process, showing that adsorption is an exothermic process and is favoured at lower temperature [5].

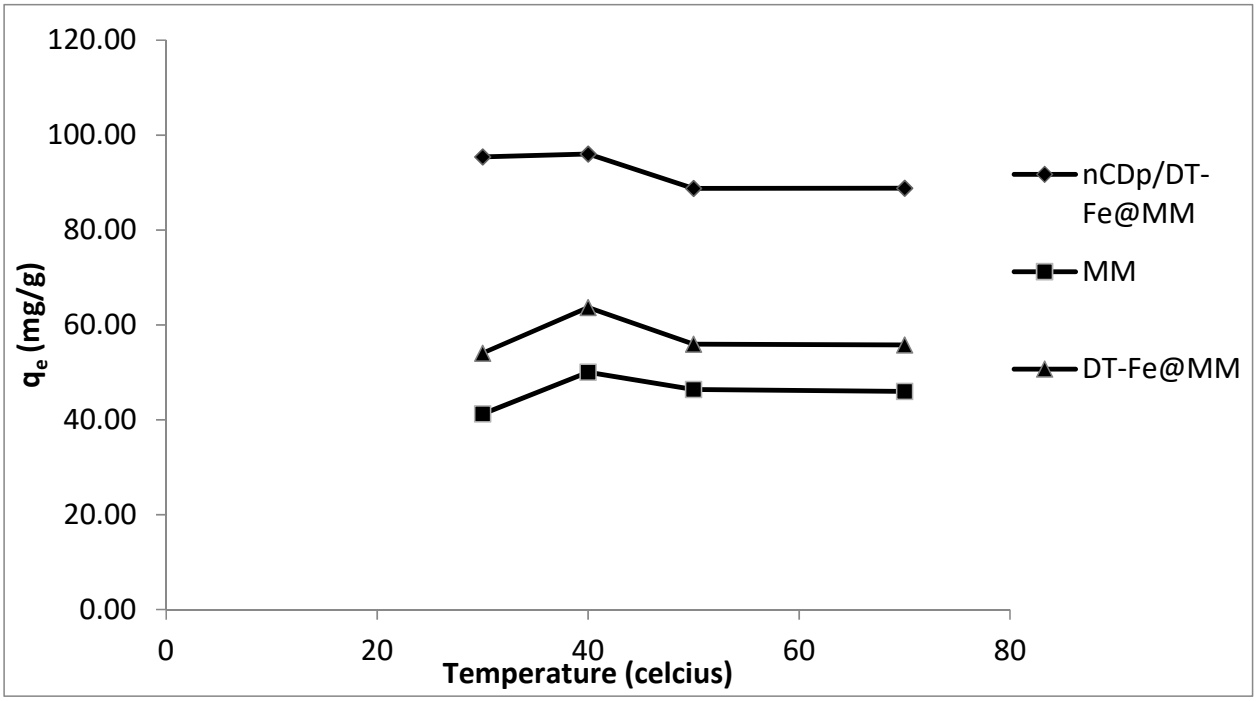

Figure 14. Effect of temperature on the removal of BPA. (Adsorption conditions: C_o = 50 mg/L; dosage = 0.02 g/L; t = 120 min; pH = 8).

3.15. Desorption Studies of BPA from Used Adsorbent

The rate of desorption of adsorbate molecules from used adsorbent was studied and the result is presented in Figure 15a,b. The rate of desorption was higher for the tripartite magnetic composite than the conventional doped titanium composite and much lower for natural montmorillonite. Rate of desorption was comparably higher in acetone as eluent compared to the DI water. Also, high rate of desorption in the tripartite magnetic composite in both eluents suggests increased pore volume and high surface area and possible application as reusable adsorbent in waste water treatment plants [63]. Acetone was a better solvent for BPA and can be used for regeneration of used adsorbent and enhance reuse. [13,53].

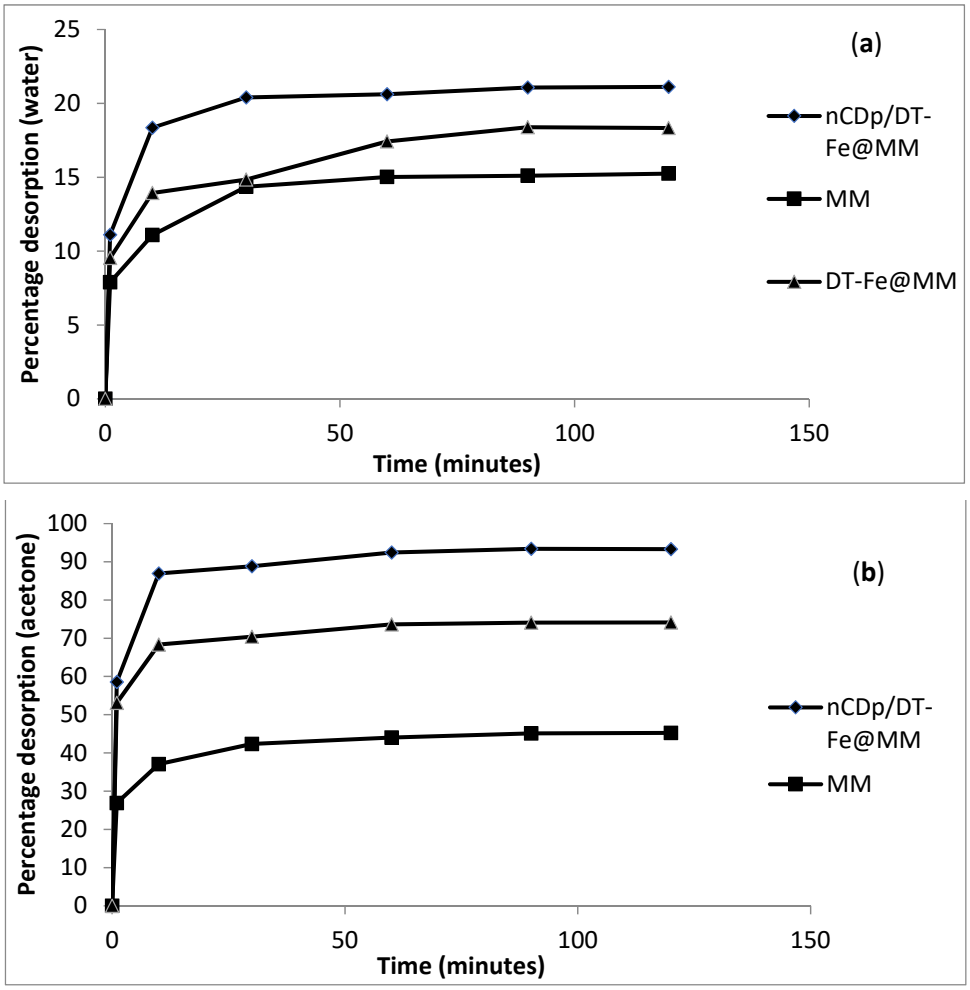

Figure 15. (**a**,**b**) Rate of desorption of BPA from used adsorbent residue using DI water and acetone. (Desorption conditions: volume of DI water; 40 mL; dosage = 0.02 g/L; t = 1–120 min; pH = 8).

3.16. Adsorption Isotherms Analysis

Adsorption isotherms can be applied to study the behaviour of adsorbate on adsorbent. Adsorption data can be subjected to various isotherm models which are useful in explaining the mechanism of the process [64]. Langmuir isotherm has been applied by Men et al. [5]. Israel et al. used Freundlich and Flory-Huggins model to study behaviour of modified coir extract on adsorption of zinc and copper from industrial effluents [62].

Langmuir model was applied to this study to access the surface coverage and adsorbent-adsorbate interaction in terms of layers of coverage. The isotherm fitting is presented in Figure S2 (Supplementary Material) and the isotherm parameters for the adsorption process are presented in Table 1. The linear form of the Langmuir equation and the Langmuir dimensionless constant equation are presented below.

$$\frac{C_e}{q_e} = \frac{1}{Q_o b} + \frac{C_e}{Q_o} \quad (3)$$

$$K_L = \frac{1}{1 + bC_o} \quad (4)$$

where C_o, C_e and q_e are initial, equilibrium concentration and adsorption capacity of BPA on adsorbent, respectively, Q_o is the theoretical maximum adsorption capacity, b is the constant of the Langmuir isotherm model and K_L is the Langmuir dimensionless constant. From the Langmuir isotherm plot, it was found that the correlation coefficients were low for the adsorption process, showing that the process could not be described completely

by the model. However, the model fits could be used to describe the process to some extent as a monolayer adsorption process. The process can further be described by the Langmuir dimensionless constant K_L, which, according to Israel et al., could provide a hint on how favourable the adsorption process was [62]. From our study and the Langmuir fitting parameter presented in Table 2, it was found that $0 < K_L < 1$ was computed for the three adsorbents; hence, the adsorption process was favourable for the unmodified montmorillonite and the functionalized composites.

Table 2. Isotherm parameters for adsorption of BPA on functionalized montmorillonite.

Adsorbents	Langmuir				Freundlich			Flory-Huggins				Dubinin-Radushkevich		
	K_L	q_m	b	R^2	K_F	1/n	R^2	K_{FH}	α_{FH}	ΔG°	R^2	q_m	E_a	R^2
MM	0.21	12.34	0.070	0.858	1.191	1.306	0.954	1.143	1.301	−336.70	0.851	1.89	270.27	0.793
DT-Fe@MM	0.22	15.55	0.072	0.892	1.104	1.332	0.959	1.236	1.438	−533.76	0.972	17.62	222.22	0.847
nCDp/DT-Fe@MM	0.25	25.44	0.080	0.916	1.412	1.273	0.957	1.770	1.208	−1438.38	0.931	18.86	220.22	0.687

Freundlich isotherm model was applied to determine heterogeneity of adsorbent surface for multilayer coverage. The Freundlich isotherm fitting is presented in Figure S3 (Supplementary Material), and the isotherm parameters for the adsorption process are presented in Table 1. The linear form of the model equation is given by the formula below.

$$\log q_e = \frac{1}{n} \mathrm{Log} C_e + \mathrm{Log}\ K_F \quad (5)$$

where K_F is the affinity coefficient of the Freundlich isotherm model and n is the constant of the Freundlich isotherm. C_e and q_e have the same meaning as in the Langmuir isotherm model. From the results, it was found that the adsorption data were best fitted into the Freundlich model with higher correlation coefficients R^2, which were 0.954, 0.959 and 0.957 respectively for the unmodified clay, doped titanium composite and the tripartite magnetic composite, respectively. This implies that the adsorption process was multilayer with adsorbate molecules filling the uneven sites on the adsorbent surfaces [5,34,65].

The Flory–Huggins isotherm has been used to describe the sorption of adsorbate on adsorbents and the result is presented in Figure S4 (Supplementary Material) and the isotherm parameters for the adsorption process are presented in Table 1. This model, which helps to account for the degree of surface coverage characteristics of the adsorbate on the adsorbents, is expressed in a linear form as

$$\mathrm{Log}\ \theta/C_o = \log K_{FH} + \alpha_{FH} \log (1 - \theta) \quad (6)$$

where θ is the surface converge of the adsorbents by the adsorbate $\theta = (1 - C_o/C_e)$. K_{FH} and α_{FH} are equilibrium constants of the Flory–Huggins isotherm model. C_o and C_e are the initial and equilibrium concentration of BPA in the simulated effluent respectively.

The equilibrium constant K_{FH} from the Flory–Huggins model is related to the Gibb's free energy using Equation (7).

$$\Delta G^\circ = RT/n\ K_{FH} \quad (7)$$

where R is the universal gas constant = 8.314 $JK^{-1}mol^{-1}$, T is the absolute temperature (°K) and K_{FH} is the Flory–Huggins's equilibrium constant. From the correlation coefficients in the model, it was found that the adsorption could be relative described by the model and that the adsorbent has high surface coverage. The standard Gibb's free energy computed for the adsorbents showed that the adsorption processes were favorably spontaneous with highly negative energy values of −336.70, −533.76 and −1438.38 KJ/mol, respectively, for the unmodified montmorillonite, doped titanium composite and the tripartite magnetic composite. It was also found that the tripartite magnetic composite has the least Gibb's free energy, and hence the most favourable and spontaneous process occurred with this adsorbent. This is due to the presence of some functional groups that facilitate the adsorp-

tion process during its modification. Men et al. and Cao et al. reported similar results for organically modified clays of different origins [5,33].

The Dubinin–Radushkevich isotherm model, which describes the uneven adsorbent surface and pore adsorption, was also used to study the adsorption process of BPA on the functionalized montmorillonite. The isotherm fitting is presented in Figure S5 (Supplementary Material), and the isotherm parameters for the adsorption process are presented in Table 1. The linear form of the model equations is shown as follows:

$$\ln q_e = \ln q_m - \beta \varepsilon^2 \quad (8)$$

$$\varepsilon = RT\ln\left(\frac{1 + C_e}{C_o}\right) \quad (9)$$

where ε is the adsorption potential energy of the Polanyi, C_o, C_e and q_m have the same meaning as in Langmuir model and β (mol^2/J^2) is the constant of the Dubinin–Radushkevish model and is related to the activation energy of the adsorption process by the following equation:

$$E_a = \frac{1}{\sqrt{2\beta}} \quad (10)$$

From the results and the model fittings, it was found that the process produces linear fittings with low correlation coefficients, thus showing that the adsorption data were not best fitted into the Dubinin–Radushkevich model. Also, the activation energy was computed for each process, and it was found that the tripartite magnetic composite had the least activation energy (220.22) compared to raw montmorillonite (270.27) and titanium doped composite (222.22), thus showing the readiness and ease of adsorption by the tripartite magnetic composite [34,62]. The summary of BPA adsorption capacity of the adsorbents as compared to those in literature is presented in Table 3.

Table 3. Summary of BPA adsorption capacity of the adsorbents as compared to those in literature.

Adsorbent	Adsorption Capacity (mg/g)	Reference
MM	12.34	This study
DT-Fe@MM	15.55	This study
nCDp/DT-Fe@MM	25.44	This study
Organo-Arizona Mont.	151.52	Zheng et al. [66]
Natural Sericite	4.816	Tiwari et al. [39]
Aluminium modified Sericite	5.047	Tiwari et al. [39]
Natural bentonite	4.816	Li et al. [37]
HTAB modified Bentonite	10.449	Li et al. [37]
EGIS/CPAB modified bentonite	119.88	Men et al. [5]
CST modified Bentonite	77.36	Cao et al. [33]

3.17. Adsorption Kinetics Model Analysis

Adsorption kinetics models reveal the effect of time on different adsorption processes. It provides theoretical insight into the mechanism of the adsorption process. In this study, the experimental data for the adsorption of BPA onto functionalized montmorillonite, raw montmorillonite and activated carbon were fitted into the pseudo-first-order kinetic model, pseudo-second-order kinetic model and intra-particle diffusion model [5,67].

The Pseudo-first-order kinetic model assumes single diffusion of adsorbate on an adsorbent surface and also assumes that adsorption is proportional to adsorbate initial concentration. Pseudo-first-order model adsorption processes are mainly characterized by physisorption. The model equation can be stated as follows:

$$\mathrm{Log}(q_e - q_t) = \log q_e - K_1 t \quad (11)$$

where K_1 is the rate constant of the pseudo-first-order kinetic model, q_e and q_t represent adsorption capacity of BPA adsorbed at time t and at equilibrium, respectively. The model fitting is presented in Figure S6 (Supplementary Material), and the model parameters are presented in Table 4. The low correlation coefficient from the model fittings shows that the adsorption process could not be effectively described by the pseudo-first-order kinetic model and that the process was not a physisorption one [68].

Table 4. Kinetic models fitting parameters for adsorption of BPA on functionalized montmorillonite.

Adsorbents	$q_{e,exp}$	Pseudo-First-Order			Pseudo-Second-Order			Intra-Particle Diffusion		
		K_1	$q_{e,cal}$	R^2	K_2	$q_{e,cal}$	R^2	K_{id}	C	R^2
MM	21.17	0.012	2.20	0.239	2.232	23.095	0.999	0.722	14.71	0.628
DT-Fe@MM	22.94	0.012	2.30	0.268	1.907	22.989	0.999	0.691	16.73	0.650
nCDp/DT-Fe@MM	23.52	0.03	38.63	0.749	2.317	23.584	0.999	0.575	18.34	0.624

The Pseudo-second-order kinetic model can be applied to describe the relationship between rate of adsorption and the square of the unoccupied sites on the adsorbent during the adsorption process. The model equation is expressed in Equation (12):

$$t/q_t = \frac{1}{k_2 q_e^2} + t/q_e \quad (12)$$

where K_2 (min^{-1}) is the rate constant of the pseudo-second-order, q_e and q_t have the same meaning as in pseudo-first-order model. The model fitting is presented in Figure S7 (Supplementary Material) and the model parameters are presented in Table 2. The model fittings showed that the adsorption process could be perfectly described by the pseudo-second-order model and that the process was chemisorption with the model correlation coefficients at 0.9999 for all adsorbents under study. Men et al. reported similar fittings for an organically modified bentonite [5].

The intra-particle diffusion model is used to describe the diffusion of adsorbates through the pore structure of the adsorbent. If the model fitting gives a straight-line graph from origin, then the process could be described by intra-particle diffusion. Conversely, it would imply that there were other processes responsible for the adsorption. The intra-particle model equation can be expressed as presented in Equation (13):

$$q_t = K_{id}\sqrt{t} + C \quad (13)$$

where K_{id} ($mg/(g.min^{0.5})$) is the rate constant of the intra-particle diffusion model, C (mg/g) represents constant related to the thickness of the boundary layer. The model fitting line is presented in Figure S8 (Supplementary Material), and the model parameters are presented in Table 2. The intra-particle diffusion model recorded low correlation coefficients for all adsorbent and indicated that the process could not be described as intra-particle diffusion as the only rate limiting mechanism but occurred by other mechanisms. Similar results have been reported for modified coir extract, modified montmorillonite and modified bentonite [3,5,62].

The Boyd model is used to predict the actual rate-determining step in the adsorption process. The Boyd model expression is represented by Equation (14). The plot of Bt against time (Figure S9) indicates that the rate of adsorption for the adsorbents was governed by the film-diffusion step.

$$\frac{q_t}{q_e} = 1 + \frac{6}{\pi^2}\sum_{n=0}^{\infty}\frac{1}{n}\exp\left(n^2 B_t\right) \quad (14)$$

3.18. Adsorption Thermodynamics Analysis

The temperature of adsorption process is related to its energetics and greatly influences the outcome of the process. The adsorption of BPA unto engineered montmorillonite was

observed at 303, 313, 323 and 343 K. The standard enthalpy change (ΔH°) and standard entropy change (ΔS°) were obtained from the van't Hoff equation and then the standard Gibb's free energy change (ΔG°) were calculated. The equations can be expressed as:

$$\ln K_d = \frac{\Delta S^\circ}{R} - \frac{\Delta H^\circ}{RT} \quad (15)$$

$$\Delta G^\circ = -RT\ln K_d \quad (16)$$

$$K_d = \frac{q_e}{C_e} \quad (17)$$

where K_d (L/mg) is the thermodynamic equilibrium constant, T (K) is the absolute temperature, R, C_e and q_e have the same meaning with other models. The plot of $\ln K_d$ against 1/T for the adsorption of BPA unto the functionalized montmorillonite is presented in Figure S10 (Supplementary Material) and the model parameters are presented in Table 5.

Table 5. Thermodynamic parameters for the adsorption of BPA on functionalized montmorillonite.

Adsorbents	ΔH°(KJ/mol)	ΔS°(J/(mol.K))	ΔG°(KJ/mol)			
			303 K	313 K	323 K	343 K
MM	−34.48	−1.679	−45.923	−50.977	−34.346	−35.908
DT-Fe@MM	−42.95	−1.902	−44.280	−50.050	−33.322	−35.591
nCDp/DT-Fe@MM	−107.73	−4.728	−58.214	−63.940	−36.512	−38.601

From the thermodynamic fitting parameters, it was found that the process was exothermic and favoured at low temperature with negative change in standard enthalpy (ΔH°), the degree of randomness decreases with a decrease in the standard entropy value (ΔS°), as the adsorption proceeds and that the adsorption processes were spontaneous at all temperatures, but most favored at 313 K with the highest negative value for the standard Gibb's free energy (ΔG°). Similar results have been previously reported [5,67,68].

4. Conclusions

In conclusion, adsorptions were effective for unmodified and modified adsorbents. However, the functionalized adsorbents showed better efficiencies under all conditions, with more favourable energetics data and high stability as indicated by their zeta potentials. The textural properties of the materials reveal larger S_{BET} for the modified composites and hence higher adsorption capacities. It could be concluded from our study that modifications were effective in adding appropriate functional group(s) to the montmorillonite to enhance the adsorption process and high BPA uptake. The magnetic property of the modified composites enhances the separation of the adsorbent form the treatment plant using an external magnetic field, thus preventing secondary pollution. Moreover, from the photodegradation studies, it was noted that the modified adsorbents exhibited high photodegradation, thus enhancing reuse of the adsorbent after already being used a few times prior. The adsorption capacity of the adsorbents increased in the order 12.34 < 15.55 < 25.44, which implies that the tripartite magnetic composite will have the highest pollutant uptake, followed by the titanium doped composite and the unmodified composite.

Supplementary Materials: The following are available online at https://www.mdpi.com/article/10.3390/pollutants2030025/s1, Figure S1. UV-visible absorbance to concentration plot for the BPA at 278 cm^{-1}, Figure S2. Langmuir isotherm model fitting for adsorption of BPA on different adsorbents (Adsorption conditions: Initial Conc. 10–50 mg/L; dosage = 0.02 g/L; t = 120 min; pH = 8), Figure S3. Freundlich isotherm model fitting for adsorption of BPA on different adsorbents (Adsorption conditions: Initial Conc. 10–50 mg/L; dosage = 0.02 g/L; t = 120 min; pH = 8), Figure S4. Flory–Huggins isotherm model fitting for adsorption of BPA on different adsorbents (Adsorption conditions: Initial Conc. 10–50 mg/L; dosage = 0.02 g/L; t = 120 min; pH = 8), Figure S5. Dubinin Radushkevich isotherm model fitting for adsorption of BPA on different adsorbents (Adsorption

conditions: Initial Conc. 10–50 mg/L; dosage = 0.02 g/L; t = 120 min; pH = 8), Figure S6. Pseudo-first-order kinetic model fitting for adsorption of BPA on different adsorbents (Adsorption conditions: Initial Conc. 10–50 mg/L; dosage = 0.02g/L; t = 120 min; pH = 8), Figure S7. Pseudo-second-order kinetic model fitting for adsorption of BPA on different adsorbents (Adsorption conditions: Initial Conc. 10–50 mg/L; dosage = 0.02 g/L; t = 120 min; pH = 8), Figure S8. Intra-particle diffusion kinetic model fitting for adsorption of BPA on different adsorbents (Adsorption conditions: Initial Conc. 10–50 mg/L; dosage = 0.02 g/L; t = 120 min; pH = 8), Figure S9. Boyd model plot for unmodified and modified montmorillonite adsorbents at 50 mg/L adsorbate concentration. Figure S10. Thermodynamic model fitting for adsorption of BPA on different adsorbents (Adsorption conditions: Initial Conc. 10–50 mg/L; dosage = 0.02 g/L; t = 120.

Author Contributions: Conceptualization, O.E.O., N.-A.O.O. and E.J.I.; methodology, O.E.O.; validation, O.E.O. and N.-A.O.O.; formal analysis, O.E.O.; investigation, O.E.O.; resources, O.E.O., E.J.I. and U.D.A.; data curation, O.E.O.; writing—original draft preparation, O.E.O.; writing—review and editing, O.E.O., N.-A.O.O., E.J.I. and U.D.A.; visualization, O.E.O. and N.-A.O.O.; supervision, E.J.I. and U.D.A. All authors have read and agreed to the published version of the manuscript.

Funding: This research received no external funding.

Institutional Review Board Statement: Not applicable.

Informed Consent Statement: Not applicable.

Data Availability Statement: Data is contained within the article or Supplementary Material.

Acknowledgments: O.E.O. acknowledges the technical support received from collaborators at King Fahd University of Petroleum & Minerals, Kingdom of Saudi Arabia during his PhD research work.

Conflicts of Interest: The authors declare no conflict of interest.

References

1. Bao, T.; Damtie, M.M.; Hosseinzadeh, A.; Wei, W.; Jin, J.; Phong Vo, H.N.; Ye, J.S.; Liu, Y.; Wang, X.F.; Yu, Z.M.; et al. Bentonite-supported nano zero-valent iron composite as a green catalyst for bisphenol A degradation: Preparation, performance, and mechanism of action. *J. Environ. Manag.* **2020**, *260*, 110105. [CrossRef]
2. Offiong, N.-A.O.; Inam, E.J.; Etuk, H.S.; Ebong, G.A.; Inyangudoh, A.I.; Addison, F. Trace Metal Levels and Nutrient Characteristics of Crude Oil-Contaminated Soil Amended with Biochar–Humus Sediment Slurry. *Pollutants* **2021**, *1*, 119–126. [CrossRef]
3. Wang, Y.; Chi, B.; Li, M.; Wei, W.; Wang, Y.; Chen, D. Synthesis of sulfonated polystyrene sphere based magnesium silicate and its selective removal for bisphenol A. *Surf. Interfaces* **2019**, *14*, 9–14. [CrossRef]
4. Tan, X.; Wan, Y.; Huang, Y.; He, C.; Zhang, Z.; He, Z.; Hu, L.; Zeng, J.; Shu, D. Three-dimensional MnO2 porous hollow microspheres for enhanced activity as ozonation catalysts in degradation of bisphenol A. *J. Hazard. Mater.* **2017**, *321*, 162–172. [CrossRef]
5. Men, X.; Guo, Q.; Meng, B.; Ren, S.; Shen, B. Adsorption of bisphenol A in aqueous solution by composite bentonite with organic moity. *Microporous Mesoporous Mater.* **2020**, *308*, 110450. [CrossRef]
6. López-Ramón, M.V.; Ocampo-Pérez, R.; Bautista-Toledo, M.I.; Rivera-Utrilla, J.; Moreno-Castilla, C.; Sánchez-Polo, M. Removal of bisphenols A and S by adsorption on activated carbon clothes enhanced by the presence of bacteria. *Sci. Total Environ.* **2019**, *669*, 767–776. [CrossRef]
7. Offiong, N.-A.O.; Inam, E.J.; Edet, J.B. Preliminary Review of Sources, Fate, Analytical Challenges and Regulatory Status of Emerging Organic Contaminants in Aquatic Environments in Selected African Countries. *Chem. Africa* **2019**, *2*, 573–585. [CrossRef]
8. Laing, L.V.; Viana, J.; Dempster, E.L.; Trznadel, M.; Trunkfield, L.A.; Uren Webster, T.M.; van Aerle, R.; Paull, G.C.; Wilson, R.J.; Mill, J.; et al. Bisphenol A causes reproductive toxicity, decreases dnmt1 transcription, and reduces global DNA methylation in breeding zebrafish (Danio rerio). *Epigenetics* **2016**, *11*, 526–538. [CrossRef] [PubMed]
9. Tsai, W.T. Human health risk on environmental exposure to bisphenol-A: A review. *J. Environ. Sci. Health Part C Environ. Carcinog. Ecotoxicol. Rev.* **2006**, *24*, 225–255. [CrossRef]
10. Wu, N.C.; Seebacher, F. Effect of the plastic pollutant bisphenol A on the biology of aquatic organisms: A meta-analysis. *Glob. Chang. Biol.* **2020**, *26*, 3821–3833. [CrossRef] [PubMed]
11. Miah, M.; Iqbal, Z.; Lai, E.P.C. Comparative Binding of Endocrine Disrupting Compounds and Pharmaceuticals with Polydopamine- and Polypyrrole-coated Magnetic Nanoparticles. *CLEAN Soil Air Water* **2015**, *43*, 173–181. [CrossRef]
12. Acosta, R.; Nabarlatz, D.; Sánchez-Sánchez, A.; Jagiello, J.; Gadonneix, P.; Celzard, A.; Fierro, V. Adsorption of Bisphenol A on KOH-activated tyre pyrolysis char. *J. Environ. Chem. Eng.* **2018**, *6*, 823–833. [CrossRef]
13. Xu, Y.; Khan, M.A.; Wang, F.; Xia, M.; Lei, W. Novel multi amine-containing Gemini surfactant modified montmorillonite as adsorbents for removal of phenols. *Appl. Clay Sci.* **2018**, *162*, 204–213. [CrossRef]

14. Onaizi, S.A.; Alshabib, M. The degradation of bisphenol A by laccase: Effect of biosurfactant addition on the reaction kinetics under various conditions. *Sep. Purif. Technol.* **2021**, *257*, 117785. [CrossRef]
15. Zhao, L.; Ji, Y.; Kong, D.; Lu, J.; Zhou, Q.; Yin, X. Simultaneous removal of bisphenol A and phosphate in zero-valent iron activated persulfate oxidation process. *Chem. Eng. J.* **2016**, *303*, 458–466. [CrossRef]
16. Sharma, J.; Mishra, I.M.; Dionysiou, D.D.; Kumar, V. Oxidative removal of Bisphenol A by UV-C/peroxymonosulfate (PMS): Kinetics, influence of co-existing chemicals and degradation pathway. *Chem. Eng. J.* **2015**, *276*, 193–204. [CrossRef]
17. Torres, R.A.; Pétrier, C.; Combet, E.; Moulet, F.; Pulgarin, C. Bisphenol A Mineralization by Integrated Ultrasound-UV-Iron (II) Treatment. *Environ. Sci. Technol.* **2007**, *41*, 297–302. [CrossRef]
18. Xie, Y.; Li, P.; Zeng, Y.; Li, X.; Xiao, Y.; Wang, Y.; Zhang, Y. Thermally treated fungal manganese oxides for bisphenol A degradation using sulfate radicals. *Chem. Eng. J.* **2018**, *335*, 728–736. [CrossRef]
19. Colombo, A.; Cappelletti, G.; Ardizzone, S.; Biraghi, I.; Bianchi, C.L.; Meroni, D.; Pirola, C.; Spadavecchia, F. Bisphenol A endocrine disruptor complete degradation using TiO_2 photocatalysis with ozone. *Environ. Chem. Lett.* **2012**, *10*, 55–60. [CrossRef]
20. Thiruvenkatachari, R.; Ouk Kwon, T.; Shik Moon, I. Application of Slurry Type Photocatalytic Oxidation-Submerged Hollow Fiber Microfiltration Hybrid System for the Degradation of Bisphenol A (BPA). *Sep. Sci. Technol.* **2005**, *40*, 2871–2888. [CrossRef]
21. Xiao, K.; Liang, H.; Chen, S.; Yang, B.; Zhang, J.; Li, J. Enhanced photoelectrocatalytic degradation of bisphenol A and simultaneous production of hydrogen peroxide in saline wastewater treatment. *Chemosphere* **2019**, *222*, 141–148. [CrossRef]
22. Mei, P.; Wang, H.; Guo, H.; Zhang, N.; Ji, S.; Ma, Y.; Xu, J.; Li, Y.; Alsulami, H.; Alhodaly, M.S.; et al. The enhanced photodegradation of bisphenol A by TiO_2/C_3N_4 composites. *Environ. Res.* **2020**, *182*, 109090. [CrossRef] [PubMed]
23. Gong, Y.; Zhao, X.; Zhang, H.; Yang, B.; Xiao, K.; Guo, T.; Zhang, J.; Shao, H.; Wang, Y.; Yu, G. MOF-derived nitrogen doped carbon modified g-C_3N_4 heterostructure composite with enhanced photocatalytic activity for bisphenol A degradation with peroxymonosulfate under visible light irradiation. *Appl. Catal. B Environ.* **2018**, *233*, 35–45. [CrossRef]
24. Alshabib, M.; Onaizi, S.A. Enzymatic Remediation of Bisphenol A from Wastewaters: Effects of Biosurfactant, Anionic, Cationic, Nonionic, and Polymeric Additives. *Water Air Soil Pollut.* **2020**, *231*, 428. [CrossRef]
25. Liu, N.; Liang, G.; Dong, X.; Qi, X.; Kim, J.; Piao, Y. Stabilized magnetic enzyme aggregates on graphene oxide for high performance phenol and bisphenol A removal. *Chem. Eng. J.* **2016**, *306*, 1026–1034. [CrossRef]
26. Chmayssem, A.; Taha, S.; Hauchard, D. Scaled-up electrochemical reactor with a fixed bed three-dimensional cathode for electro-Fenton process: Application to the treatment of bisphenol A. *Electrochim. Acta* **2017**, *225*, 435–442. [CrossRef]
27. Zbair, M.; Ainassaari, K.; Drif, A.; Ojala, S.; Bottlinger, M.; Pirilä, M.; Keiski, R.L.; Bensitel, M.; Brahmi, R. Toward new benchmark adsorbents: Preparation and characterization of activated carbon from argan nut shell for bisphenol A removal. *Environ. Sci. Pollut. Res.* **2018**, *25*, 1869–1882. [CrossRef] [PubMed]
28. Skaf, D.W.; Punzi, V.L.; Rolle, J.T.; Kleinberg, K.A. Removal of micron-sized microplastic particles from simulated drinking water via alum coagulation. *Chem. Eng. J.* **2020**, *386*, 123807. [CrossRef]
29. Staroń, P.; Chwastowski, J. Raphia-Microorganism Composite Biosorbent for Lead Ion Removal from Aqueous Solutions. *Materials* **2021**, *14*, 7482. [CrossRef]
30. Kum, H.; Kim, M.K.; Choi, H.T. Degradation of endocrine disrupting chemicals by genetic transformants in Irpex lacteus with an inducible laccase gene of Phlebia tremellosa. *Biodegradation* **2009**, *20*, 673–678. [CrossRef]
31. Sakai, K.; Yamanaka, H.; Moriyoshi, K.; Ohmoto, T.; Ohe, T. Biodegradation of Bisphenol A and Related Compounds by Sphingomonas sp. Strain BP-7 Isolated from Seawater. *Biosci. Biotechnol. Biochem.* **2007**, *71*, 51–57. [CrossRef] [PubMed]
32. Verma, B.; Balomajumder, C. Hexavalent chromium reduction from real electroplating wastewater by chemical precipitation. *Bull. Chem. Soc. Ethiop.* **2020**, *34*, 67–74. [CrossRef]
33. Cao, Y.; Zhou, G.; Zhou, R.; Wang, C.; Chi, B.; Wang, Y.; Hua, C.; Qiu, J.; Jin, Y.; Wu, S. Green synthesis of reusable multifunctional γ-Fe_2O_3/bentonite modified by doped TiO_2 hollow spherical nanocomposite for removal of BPA. *Sci. Total Environ.* **2020**, *708*, 134669. [CrossRef] [PubMed]
34. Lin, X.; Huang, Q.; Qi, G.; Xiong, L.; Huang, C.; Chen, X.; Li, H.; Chen, X. Adsorption behavior of levulinic acid onto microporous hyper-cross-linked polymers in aqueous solution: Equilibrium, thermodynamic, kinetic simulation and fixed-bed column studies. *Chemosphere* **2017**, *171*, 231–239. [CrossRef] [PubMed]
35. Xu, X.; Chen, W.; Zong, S.; Ren, X.; Liu, D. Magnetic clay as catalyst applied to organics degradation in a combined adsorption and Fenton-like process. *Chem. Eng. J.* **2019**, *373*, 140–149. [CrossRef]
36. Rathnayake, S.I.; Xi, Y.; Frost, R.L.; Ayoko, G.A. Environmental applications of inorganic–organic clays for recalcitrant organic pollutants removal: Bisphenol A. *J. Colloid Interface Sci.* **2016**, *470*, 183–195. [CrossRef]
37. Li, Y.; Jin, F.; Wang, C.; Chen, Y.; Wang, Q.; Zhang, W.; Wang, D. Modification of bentonite with cationic surfactant for the enhanced retention of bisphenol A from landfill leachate. *Environ. Sci. Pollut. Res.* **2015**, *22*, 8618–8628. [CrossRef] [PubMed]
38. Garikoé, I.; Sorgho, B.; Yaméogo, A.; Guel, B.; Andala, D. Removal of bisphenol A by adsorption on organically modified clays from Burkina Faso. *Bioremediat. J.* **2021**, *25*, 22–47. [CrossRef]
39. Tiwari, D.; Lee, S.M.; Thanhmingliana, T. Hybrid materials in the decontamination of bisphenol A from aqueous solutions. *RSC Adv.* **2014**, *4*, 43921–43930. [CrossRef]

40. Sasai, R.; Sugiyama, D.; Takahashi, S.; Tong, Z.; Shichi, T.; Itoh, H.; Takagi, K. The removal and photodecomposition of n-nonylphenol using hydrophobic clay incorporated with copper-phthalocyanine in aqueous media. *J. Photochem. Photobiol. A Chem.* **2003**, *155*, 223–229. [CrossRef]
41. Alani, O.A.; Ari, H.A.; Offiong, N.-A.O.; Alani, S.O.; Li, B.; Zeng, Q.; Feng, W. Catalytic Removal of Selected Textile Dyes Using Zero-Valent Copper Nanoparticles Loaded on Filter Paper-Chitosan-Titanium Oxide Heterogeneous Support. *J. Polym. Environ.* **2021**, *29*, 2825–2839. [CrossRef]
42. Ari, H.A.; Alani, O.A.; Zeng, Q.; Ugya, Y.A.; Offiong, N.-A.O.; Feng, W. Enhanced UV-assisted Fenton performance of nanostructured biomimetic α-Fe2O3 on degradation of tetracycline. *J. Nanostructure Chem.* **2022**, *12*, 45–58. [CrossRef]
43. Alani, O.A.; Ari, H.A.; Alani, S.O.; Offiong, N.-A.O.; Feng, W. Visible-Light-Driven Bio-Templated Magnetic Copper Oxide Composite for Heterogeneous Photo-Fenton Degradation of Tetracycline. *Water* **2021**, *13*, 1918. [CrossRef]
44. Amari, A.; Mohammed Alzahrani, F.; Mohammedsaleh Katubi, K.; Salem Alsaiari, N.; Tahoon, M.A.; Ben Rebah, F. Clay-Polymer Nanocomposites: Preparations and Utilization for Pollutants Removal. *Materials* **2021**, *14*, 1365. [CrossRef]
45. Unuabonah, E.I.; Taubert, A. Clay–polymer nanocomposites (CPNs): Adsorbents of the future for water treatment. *Appl. Clay Sci.* **2014**, *99*, 83–92. [CrossRef]
46. Pavlidou, S.; Papaspyrides, C.D. A review on polymer–layered silicate nanocomposites. *Prog. Polym. Sci.* **2008**, *33*, 1119–1198. [CrossRef]
47. Sternik, D.; Galaburda, M.V.; Bogatyrov, V.M.; Oranska, O.I.; Charmas, B.; Gun'ko, V.M. Novel porous carbon/clay nanocomposites derived from kaolinite/resorcinol-formaldehyde polymer blends: Synthesis, structure and sorption properties. *Appl. Surf. Sci.* **2020**, *525*, 146361. [CrossRef]
48. Okon, O.E.; Israel, A.U.; Inam, E.J.; Etim, U.J. Preparation and characterization of Fe2O3/mesoporous clay composite from Nigerian local bentonite clay. *J. Mater. Environ. Sci.* **2019**, *10*, 618–623. [CrossRef]
49. Liu, C.; Wu, P.; Tran, L.; Zhu, N.; Dang, Z. Organo-montmorillonites for efficient and rapid water remediation: Sequential and simultaneous adsorption of lead and bisphenol A. *Environ. Chem.* **2018**, *15*, 286–295. [CrossRef]
50. Liu, S.; Wu, P.; Chen, M.; Yu, L.; Kang, C.; Zhu, N.; Dang, Z. Amphoteric modified vermiculites as adsorbents for enhancing removal of organic pollutants: Bisphenol A and Tetrabromobisphenol A. *Environ. Pollut.* **2017**, *228*, 277–286. [CrossRef] [PubMed]
51. Middea, A.; Spinelli, L.S.; Souza Jr, F.G.; Neumann, R.; Fernandes, T.L.A.P.; Gomes, O.d.F.M. Preparation and characterization of an organo-palygorskite-Fe3O4 nanomaterial for removal of anionic dyes from wastewater. *Appl. Clay Sci.* **2017**, *139*, 45–53. [CrossRef]
52. Wang, J.; Zhang, M. Adsorption Characteristics and Mechanism of Bisphenol A by Magnetic Biochar. *Int. J. Environ. Res. Public Health* **2020**, *17*, 1075. [CrossRef] [PubMed]
53. Salehinia, S.; Ghoreishi, S.M.; Maya, F.; Cerdà, V. Hydrophobic magnetic montmorillonite composite material for the efficient adsorption and microextraction of bisphenol A from water samples. *J. Environ. Chem. Eng.* **2016**, *4*, 4062–4071. [CrossRef]
54. Bala, P.; Samantaray, B.K.; Srivastava, S.K. Dehydration transformation in Ca-montmorillonite. *Bull. Mater. Sci.* **2000**, *23*, 61–67. [CrossRef]
55. Wan, D.; Chen, Y.; Shi, Y.; Liu, Y.; Xiao, S. Effective adsorption of bisphenol A from aqueous solution over a novel mesoporous carbonized material based on spent bleaching earth. *Environ. Sci. Pollut. Res.* **2021**, *28*, 40035–40048. [CrossRef] [PubMed]
56. Schaber, P.M.; Colson, J.; Higgins, S.; Thielen, D.; Anspach, B.; Brauer, J. Thermal decomposition (pyrolysis) of urea in an open reaction vessel. *Thermochim. Acta* **2004**, *424*, 131–142. [CrossRef]
57. Batra, S.; Datta, D.; Sai Beesabathuni, N.; Kanjolia, N.; Saha, S. Adsorption of Bisphenol-A from aqueous solution using amberlite XAD-7 impregnated with aliquat 336: Batch, column, and design studies. *Process Saf. Environ. Prot.* **2019**, *122*, 232–246. [CrossRef]
58. Mustapha, S.; Ndamitso, M.M.; Abdulkareem, A.S.; Tijani, J.O.; Shuaib, D.T.; Ajala, A.O.; Mohammed, A.K. Application of TiO_2 and ZnO nanoparticles immobilized on clay in wastewater treatment: A review. *Appl. Water Sci.* **2020**, *10*, 49. [CrossRef]
59. Xiang, Y.; Gao, M.; Ding, F.; Shen, T. The efficient removal of dimethyl phthalate by three organo-vermiculites with imidazolium-based gemini surfactants in aqueous media. *Colloids Surfaces A Physicochem. Eng. Asp.* **2019**, *580*, 123726. [CrossRef]
60. Mohan, N.; Vijayalakshmi, K.P.; Koga, N.; Suresh, C.H. Comparison of aromatic NH···π, OH···π, and CH···π interactions of alanine using MP2, CCSD, and DFT methods. *J. Comput. Chem.* **2010**, *31*, 2874–2882. [CrossRef] [PubMed]
61. Park, Y.; Ayoko, G.A.; Horváth, E.; Kurdi, R.; Kristof, J.; Frost, R.L. Structural characterisation and environmental application of organoclays for the removal of phenolic compounds. *J. Colloid Interface Sci.* **2013**, *393*, 319–334. [CrossRef] [PubMed]
62. Israel, A.U.; Okon, O.E. Removal of Zinc from Aqueous Solution by Adsorption using Coir Dust (Residue and Extract). *Chem. Mater. Res.* **2014**, *6*, 154–159.
63. Awad, A.M.; Shaikh, S.M.R.; Jalab, R.; Gulied, M.H.; Nasser, M.S.; Benamor, A.; Adham, S. Adsorption of organic pollutants by natural and modified clays: A comprehensive review. *Sep. Purif. Technol.* **2019**, *228*, 115719. [CrossRef]
64. Wang, J.; Gao, M.; Shen, T.; Yu, M.; Xiang, Y.; Liu, J. Insights into the efficient adsorption of rhodamine B on tunable organo-vermiculites. *J. Hazard. Mater.* **2019**, *366*, 501–511. [CrossRef]
65. Rahardjo, A.K.; Susanto, M.J.J.; Kurniawan, A.; Indraswati, N.; Ismadji, S. Modified Ponorogo bentonite for the removal of ampicillin from wastewater. *J. Hazard. Mater.* **2011**, *190*, 1001–1008. [CrossRef] [PubMed]

66. Zheng, S.; Sun, Z.; Park, Y.; Ayoko, G.A.; Frost, R.L. Removal of bisphenol A from wastewater by Ca-montmorillonite modified with selected surfactants. *Chem. Eng. J.* **2013**, *234*, 416–422. [CrossRef]
67. Ahmed, M.B.; Zhou, J.L.; Ngo, H.H.; Johir, M.A.H.; Sun, L.; Asadullah, M.; Belhaj, D. Sorption of hydrophobic organic contaminants on functionalized biochar: Protagonist role of π-π electron-donor-acceptor interactions and hydrogen bonds. *J. Hazard. Mater.* **2018**, *360*, 270–278. [CrossRef] [PubMed]
68. Errais, E.; Duplay, J.; Darragi, F.; M'Rabet, I.; Aubert, A.; Huber, F.; Morvan, G. Efficient anionic dye adsorption on natural untreated clay: Kinetic study and thermodynamic parameters. *Desalination* **2011**, *275*, 74–81. [CrossRef]